NACA RM L57G15

NACA

RESEARCH MEMORANDUM

AN INVESTIGATION OF THE PERFORMANCE OF A SEMIELLIPTICAL

SCOOP INLET AT MACH NUMBERS OF 1.60, 1.76, AND 2.02

By Clyde Hayes and Ernest A. Mackley

Langley Aeronautical Laboratory
Langley Field, Va.

NATIONAL ADVISORY COMMITTEE
FOR AERONAUTICS
WASHINGTON
January 7, 1958

1F

NATIONAL ADVISORY COMMITTEE FOR AERONAUTICS

RESEARCH MEMORANDUM

AN INVESTIGATION OF THE PERFORMANCE OF A SEMIELLIPTICAL

SCOOP INLET AT MACH NUMBERS OF 1.60, 1.76, AND 2.02

By Clyde Hayes and Ernest A. Mackley

SUMMARY

An experimental investigation has been made of the performance of a semielliptical scoop inlet having a two-dimensional flow field at the design Mach number of 2.0. This investigation included a study of the effects of inlet-leading-edge shape and boundary-layer bleed on the pressure recovery and total-pressure distribution. The tests were run primarily at a Mach number of 2.02. One configuration, however, was also tested at Mach numbers of 1.76 and 1.60 to determine the effects of free-stream Mach number.

The use of boundary-layer bleed near the inlet throat on both the diverter side and compression side resulted in an increase of pressure recovery from 0.83 to 0.90 at Mach number 2.02 with an increase of critical mass-flow ratio of 0.05 and improvement of the total-pressure distribution in the circumferential direction. Without boundary-layer bleed, improved starting and increased pressure recovery resulted from cutting slots in the leading edge or otherwise relieving the leading edge near the diverter. Generally, however, modifications to the inlet which result in improved starting and higher pressure recovery decreased the subcritical stability range. The configuration tested at Mach numbers of 1.76 and 1.60 in addition to 2.02 showed that the effect of free-stream Mach number on the pressure recovery and entering-mass-flow ratio was small; the pressure recovery increased from 0.89 to 0.91 as the Mach number was decreased from 2.02 to 1.60.

The performance of a buzz suppressor, a device to extend the stable subcritical mass-flow range of the inlet, and of rearward-facing control tubes, designed to provide a signal for operation of bypass doors, was also investigated. The buzz suppressor was tested at Mach numbers 2.02 and 1.76 and was found to increase the stable subcritical range from 0.02 to 0.30 at Mach number 2.02 and from 0.08 to 0.24 at Mach number 1.76. The rearward-facing control tubes, located near the throat of the inlet, were tested at Mach numbers 2.02, 1.76, and 1.60 and were found to indicate the normal-shock position at Mach number 2.02; however, at Mach numbers 1.76 and 1.60, the shock position could not be precisely determined.

INTRODUCTION

The design of a rectangular supersonic scoop inlet having high pressure recovery and low drag has been reported in reference 1. A similar inlet can be designed having a semielliptical frontal cross section by tracing the streamlines bounded by this shape through a two-dimensional flow field with the use of the method described in reference 2. The resulting inlet design has the two-dimensional flow field without the structural problems of a rectangular inlet.

The inlet tested in this investigation was a wing-root adaptation of the semielliptical cross-section inlet as designed by an aircraft manufacturer. The purpose of this investigation was to develop this design into an inlet suitable for application on a specific airplane. The effect of inlet-leading-edge shape and internal boundary-layer bleed on the total-pressure recovery and distribution at the compressor-face station have been determined. Tests were made of a device to extend the stable subcritical mass-flow range of the inlet and of rearward-facing total-pressure tubes near the inlet throat to be used for control purposes.

A 1/10-scale model of the inlet was tested in a jet facility of the Langley gas dynamics laboratory at Mach numbers of 2.02, 1.76, and 1.60 at zero angle of attack and Reynolds numbers of 2.05, 2.14, and 2.26 × 10^6 per inch, respectively.

SYMBOLS

A area, sq in.

A_∞ estimated inlet projected area, 4.22 sq in.

h height of buzz suppressors, measured from diverter to outside corner, in.

M_∞ free-stream Mach number

m inlet mass flow, slugs/sec

m_b bleed mass flow, slugs/sec

m_∞ mass flow at free-stream conditions through a stream tube of cross-sectional area equal to the estimated inlet projected area, slugs/sec

p static pressure, lb/sq ft

p_c control-tube pressure, lb/sq ft

$p_{t,e}$ diffuser-exit total pressure, measured at survey rake (station 39.60), lb/sq ft

$p_{t,\infty}$ free-stream total pressure, lb/sq ft

w_a weight air flow, lb/sec

δ ratio of engine-inlet total pressure to absolute static pressure of NACA standard atmosphere at sea level

θ ratio of absolute engine-inlet total temperature to absolute static temperature of NACA standard atmosphere at sea level

DESCRIPTION OF THE MODEL

A schematic drawing of the semielliptical inlet model is shown in figure 1, and a photograph of the model and tunnel with one side wall removed is shown in figure 2. The model simulated a portion of one side of the fuselage, and was rotated so that the inlet, located at the root of the right-hand wing, was upright. All directions used herein are relative to the airplane axes in its normal attitude. The simulated fuselage ahead of the inlet was alined with the flow, and its length was such that any disturbance from the leading edge of the fuselage would miss the inlet. The forward end of the simulated fuselage formed a scoop to remove the stream tube ahead of the fuselage.

Internally, the duct was simulated back to the compressor-face station; one-half of the engine accessory housing was also simulated. Since the wing and inlet were located above the center line of the engine, the duct turned downward as well as inward to the center line. Located at the compressor-face station was a rake with 29 total-pressure tubes and 5 static-pressure tubes in the duct wall. Behind the rake, the duct turned downward and was connected through external piping to an orifice flowmeter and throttling valves, as in reference 1.

The contraction ratio of the inlet was varied by means of a movable compression surface which, in the forward positions, increased the contraction and was designed to be operated in flight according to a Mach number schedule. The area variation of the duct is shown in figure 3 for four positions of the compression surface. The change in the location of the throat of the inlet with movement of the compression surface is also indicated in figure 3. At a Mach number of 2.02, the initial compression wave occurred at the leading edge of the movable compression surface.

Ahead of this surface, the internal contour of the inlet was alined with the flow at zero angles of attack and yaw. With the compression surface in the most rearward position, there was a slight amount of compression ahead of the movable compression surface.

Details of the model are shown in figure 4. Leading edge I (fig. 4(a)) was sharp, although swept behind the shock wave from the outboard tip of the inlet at the design Mach number of 2.0. Leading edges II and III were sharp only near the outboard tip, since they were formed by cutting back leading edge I and rounding off the resulting blunt leading edge.

The two fuselage boundary-layer diverters are shown in figure 4(c). Either diverter A or B was used for all tests to divert the boundary layer on the simulated fuselage ahead of the inlet. Diverter A was designed for removal of the boundary layer on the diverter by means of a vacuum pump. Removable plates forming a portion of the inboard duct wall were used to facilitate changing the slot configurations. The compartment immediately behind the plate was connected to the external vacuum system through four tubes. The bleed-air mass flow was measured with a small flowmeter, similar to that used to measure the inlet mass flow, located in the external piping to the vacuum system. Bleed mass flow was varied by a throttling valve downstream of the flowmeter. Diverter B was designed to exhaust the diverter bleed air to the free stream. The air passed out from a small compartment beneath the diverter slots through downstream-facing exits at the rear of each side of the diverter. Since the splitter plate of diverter B was wider than that of diverter A, it was also longer to keep the same angle at the tip. Both diverters were at an angle of 4° from the vertical axis, to fit the contour of the fuselage, and canted downward $2\frac{1}{2}^\circ$ from the free-stream direction.

The boundary-layer diverter height was 0.27 inch for diverter A and 0.30 inch for diverter B. This height was based on the boundary layer calculated for the complete fuselage. Since only a small section of the fuselage was simulated in this investigation, the diverter height was unnecessarily large; however, changing the diverter height would have changed the inlet configuration. Shadowgraphs showed that the diverter height was approximately twice the boundary-layer thickness for these tests.

In this paper the inlets will be designated as to the leading edge and diverter that are being used. For example, the inlet using leading edge II with diverter B will be referred to as inlet II-B.

The slot configurations used with diverter A and the vacuum system are shown in figure 4(d). Where the slots extend ahead of the removable plate, they were cut into the duct wall. The slot configuration used with diverter B was similar in slot location to configuration 7, and is shown in figure 4(c).

The location of the slots used for boundary-layer bleed on the compression surface are shown in figure 4(e). Grooves cut into the back of the compression surface carried the bleed air from the slots to the compression-surface suction compartment. The compression-surface access door served as an exit for bleed air through external piping to the vacuum pumps. Suction on the compression surface could be used only in conjunction with diverter B.

The buzz suppressors shown in figure 4(f) were used to stabilize the normal shock ahead of the inlet and to obtain stable inlet flow at mass-flow ratios lower than the values obtainable with the basic inlet. Although in an actual installation they would be retracted and only extend at the start of buzz, for the present tests they were stationary. Each position of the buzz suppressors was simulated by soldering a set of appropriately contoured pieces to the diverter. Not shown on the drawing are small triangular braces behind the buzz suppressors for added strength needed for the tests. These were so located as to minimize interference with the perforations, and where necessary, were cut away to allow free flow of air through the perforations.

Details of the control tubes, which were used to obtain a signal for operation of bypass doors, are shown in figure 4(g). These were installed on the inboard wall of the duct and were located on the portion of the duct that was removable with the diverter. The tubes face downstream and were staggered to minimize interference with each other.

PROCEDURE

Most of the tests were run at a Mach number of 2.02. Tests of leading edge III with diverter B (inlet III-B) were also made at Mach numbers of 1.76 and 1.60. All tests were made at zero angles of attack and yaw, and only pressure and mass-flow measurements were made.

Measurements of the settling-chamber pressure and static pressure at the inlet flowmeter were made using Bourdon tube gages. The pressure differences across the orifices of both flowmeters were measured with tetrabromoethane-filled U-tubes. All other pressure measurements were made using mercury-filled manometers.

The total-pressure tubes of the rake at the compressor-face station were arranged in five radial rows of five tubes each, as shown in figure 1. The tubes were spaced in each radial row so that a numerical average of these 25 tubes was equivalent to area-weighting of the pressure recovery.

The mass-flow ratio through the model was calculated from the orifice data by using an inlet projected area of 4.22 square inches. Since the projected inlet frontal area increased with increasing leading-edge sweep (greater than 58°) and the rounded leading edges on these configurations made the determination of the exact amount of this increase difficult, a constant value was used for the theoretical free-stream capture area. This facilitated the comparison of mass-flow data of the various inlet configurations tested. Maximum mass-flow ratios greater than 1.0 indicate that the true area was greater than 4.22 square inches; the mass-flow ratios are therefore consistently high. This was also true of the bleed-mass-flow data, which were also based on the same projected area.

Buzz was detected by observation of the flow during the runs with a schlieren system. Since buzz in this type of inlet, and with high density flow, is readily discernable, this method of buzz detection was quite adequate.

The accuracy of the pressure recovery and mass-flow ratios were estimated to be accurate within ±2 percent.

The distortion as referred to in the discussion of the data herein is defined as the difference between the maximum and minimum local total-pressure recovery divided by the average pressure recovery.

RESULTS AND DISCUSSION

Performance of Inlets Without Boundary-Layer Bleed

The pressure recovery obtained at $M_\infty = 2.02$ with the inlet as originally designed (inlet I-A) is shown as a function of mass-flow ratio in figure 5(a). The critical pressure-recovery value of 0.72 was quite low, corresponding to normal-shock pressure recovery. Observation of the flow by means of a schlieren system indicated that at very low back pressure the inlet started, but as back pressure was increased the inlet became unstarted, with an abrupt change in the flow pattern. The shadowgraphs of figure 5(c) show the two flow patterns. This inlet could be completely started for the maximum mass-flow-ratio point only; all other data points correspond to an unstarted condition similar to that shown in the second shadowgraph. The total-pressure distribution (fig. 5(b)) was relatively flat due to the absence of a high-pressure core, usually associated with higher pressure recoveries at these Mach numbers.

The inlet was modified to configuration Ia-A, as shown in figure 4(a). A slot was cut in the leading edge in each side at the junction of the inlet and diverter. The purpose of these slots was to eliminate the

abrupt change in the forward movement of the normal shock wave with increasing back pressure by allowing spillage behind the normal shock as it moved ahead of the slots. The effect of the slots on the pressure recovery and mass flow is shown in figure 6. The critical pressure recovery was 0.81 compared with 0.72 without slots, and the mass-flow ratio decreased about 5 percent with no subcritical stability range.

An additional slot was added to the lower inlet wall normal to the free-stream direction, as shown in figure 4(a). The purpose of this slot was to bleed off some of the boundary layer building up inside the inlet and possibly to allow the normal shock to move downstream. This configuration (inlet Ib-A) showed a very small increase of pressure recovery and mass-flow ratio over that of inlet Ia-A, and like inlet Ia-A was without any subcritical stability range.

The improvements in pressure recovery obtained by the modification of leading edge I resulted in the design of leading edge II. (See fig. 4(a).) The leading edge was cut back to the downstream end of the previously cut slots, thereby increasing the sweep angle of the leading edge to 65°. The performance of this inlet (inlet II-A) is also shown in figure 6. The pressure recovery was slightly higher than the original leading-edge configuration, and the critical mass-flow ratio was decreased about 2 percent. Inlet II-A did have some subcritical stability, which was nonexistent for inlet Ia-A and inlet Ib-A.

The total-pressure distributions of inlets Ia-A, Ib-A, and II-A are presented in figure 7. The total-pressure distributions for these higher recovery inlets are not as flat as that of inlet I-A due to the presence of a high-pressure area near the center of the duct. The total-pressure distribution of all three inlets were similar, having the same maximum and minimum pressures, the only difference being small differences in the location of the high-pressure cores.

Shadowgraphs of inlets Ia-A and II-A are shown in figure 8. The shadowgraphs of inlet Ia-A indicate that for supercritical operation a normal shock is standing ahead of the downstream end of the slots instead of moving down the duct. The flow for inlet Ia-A was much cleaner near the diverter for critical operation than for inlet I-A. The shadowgraphs of inlet II-A show that the normal shock was at approximately the same location as inlet Ia-A for both supercritical and critical operation.

Effect of Diverter Boundary-Layer Bleed

The effect of diverter boundary-layer bleed on the pressure recovery and mass-flow ratio through the duct of inlets Ia-A and II-A are shown in figure 9. The diverter boundary-layer slot configurations are shown in figure 4(c). With inlet Ia-A, figure 9(a), slot configuration 1 with a bleed-mass-flow ratio of 0.03 reduced the mass-flow ratio with no change

in pressure recovery. Configurations 3, 4, and 7 increased both maximum pressure recovery and critical mass-flow ratio. The bleed-mass-flow ratio used for configuration 7 was 0.03 at low back pressure, increasing to 0.06 at maximum back pressure. The bleed-mass-flow ratios for configurations 3 and 4 are estimated at approximately the same as for configuration 7, although complete data are not available. Use of diverter bleed allowed the normal shock to move farther downstream into the inlet and gave gains in mass-flow ratio over that of inlet Ia-A without diverter bleed by reducing the spillage.

With inlet II-A, figure 9(b), the use of diverter bleed through slot configuration 3 resulted in the highest pressure recovery, almost 0.87, and the use of diverter bleed through configuration 2 resulted in the highest critical mass-flow ratio. Configurations 4 and 7 gave increases in critical mass flow over the no-bleed configuration but very little increase in pressure recovery. The subcritical stability range was greater with configurations 4 and 7 than the no-bleed configurations, whereas configurations 2 and 3 had very little subcritical stability; the absence of subcritical stability seemed to be concomitant with configurations having improved pressure recovery. The diverter bleed-mass-flow ratio for configuration was 0.04 at low back pressure and 0.05 at high back pressure; configurations 3, 4, and 7 had bleed-mass-flow ratios of 0.05 and 0.08.

Figure 9(c) shows the performance of two bleed configurations consisting of three rows of 1/16-inch-diameter holes; configuration 6 had small additional slots ahead of the holes. Gains of both pressure recovery and critical mass-flow ratio were made over the no-bleed configuration, but were not quite so good as the better of the slot-type configurations; the subcritical stability range was greater for the hole-type configurations. The bleed-mass-flow ratios for the hole-type configurations was approximately 0.02.

The total-pressure distribution at the compressor-face station for inlets Ia-A and II-A are shown in figure 10. These distributions when compared with those of figure 7 for inlets Ia-A and II-A show that, both with and without diverter boundary-layer bleed, the maximum-minus-minimum total pressure was approximately 10 percent of the average with the high pressure regions spread out circumferentially as a result of diverter suction. This effect was more pronounced for inlet II-A.

Shadowgraphs of inlet II-A with diverter boundary-layer configuration 7 are shown in figure 11. The effect of diverter bleed can be seen by comparing figure 11 with the shadowgraphs of inlet II-A without diverter bleed in figure 8. The normal shock which stood ahead of the junction of the leading edge and the diverter moved downstream into the inlet with the use of diverter bleed, and the flow entering the inlet was nearly completely supersonic.

Effect of Leading-Edge Sweep Angle

The use of an inlet having an upper leading edge of less sweep than that of the original design was contemplated in the event that adverse angle-of-attack effects were encountered with the original design. In order to check the adverse effect of additional boundary layer on the upper surface at zero angle of attack, tests were made of the inlet with diverter A and slot configuration 7 and with an upper leading edge of varying sweep. Details of the modified leading edges are shown in figure 4(b). The results of these tests, presented in figure 12, show a trend of decreasing pressure recovery and mass-flow ratio with decreasing upper-leading-edge sweep angle. Very little could be seen of the shock pattern of the entering flow; the performance, however, indicates that the additional boundary-layer buildup on the extended leading edge (sweep angle less than 58°) did not permit the inlet to become started. The 58°-65° (58° upper-leading-edge sweep and 65° lower-leading-edge sweep) inlet showed good mass-flow characteristics, the maximum mass-flow ratio being approximately the same as that of inlet II-B and thereby indicating that the inlet had started. The mass flow did not decrease as rapidly with increasing pressure recovery as for inlet II-B and was higher at the critical point. The critical pressure recovery, however, was 0.03 lower than that of inlet II-B. The inlet configuration having the lower leading-edge cutback beyond that of inlet II-B (58°-71°) showed poor performance, possibly due to excessive spillage at the lower leading edge. All configurations tested in this phase of the program resulted in a loss of pressure recovery of at least 0.02, and with the exception of the 58°-65° inlet, in losses of entering-mass-flow ratio of at least 0.02 from configuration inlet II-A with bleed slot configuration 7.

Total pressure distributions of the inlets with decreased leading-edge sweep are shown in figure 13. The distributions for the 0°-65°, 20°-65°, and 36°-65° leading edges are similar with small difference in maximum pressure recovery at the center of the duct and are similar to that of configuration II-A. The 58°-65° leading edge showed the best total-pressure distribution in both radial and circumferential directions; it was particularly good circumferentially.

Effect of Compression-Surface Bleed

The tests to determine the effect of compression-surface bleed were made with inlet II-B, details of which are shown in figure 4(c), with provisions made for diverter boundary-layer removal by discharging through exits at the top and bottom of the inlet. The diverter boundary-layer slot configuration used with diverter B, shown in figure 4(c), was similar in slot location to configuration 7 which was used with diverter A. Diverter B simulated an installation as would be used on a full-size airplane and left the vacuum system available for compression-surface

suction. Results of tests of inlet II-B with no compression-surface bleed, shown in figure 14, showed an increase in pressure recovery to 0.85, compared with 0.83 for diverter A with slot configuration 7. Since the slot configurations of diverters A and B were similar, the difference in pressure recovery would seem to be associated with the diverter shape, diverter B being wider than diverter A due to addition of boundary-layer exits at the sides. The maximum bleed-mass-flow ratio through the diverter slots for diverter B, 0.02, estimated from a static- and a total-pressure tube at each exit, was much smaller than with diverter A. During the tests with diverter A, it was observed that the normal shock could be made to move into the inlet with a very small amount of suction applied, indicating that the boundary-layer removal system would not need to be capable of handling the high bleed mass flows for diverter A to be effective.

The performance of inlet II-B with compression-surface bleed, through several compression-surface slot configurations, is shown in figure 14. The maximum pressure recovery was approximately 0.90, as compared with 0.83 for inlet II-A with no boundary-layer bleed, and 0.87 for the best diverter boundary-layer-bleed configuration. The mass-flow ratio through the duct for the seven-bleed-slot configurations was less than that for the four-slot configurations due to the increase of bleed mass flow. With suction on the seven compression-surface slots with the diverter slots closed, the pressure recovery dropped to 0.86, indicating that both diverter and compression-surface bleed are necessary to achieve maximum pressure recovery.

Figure 15 shows the peak pressure recovery for several compression-surface bleed-slot configurations. With the seven-slot configuration and with four slots of reduced length, the pressure recovery drops off at a bleed-mass-flow ratio of approximately 0.06; with the basic four-slot configuration the drop was at approximately 0.075. It should be noted that the values of peak pressure recovery obtained with configurations at zero suction are lower than the peak pressure recovery from the tests with no-bleed slots. Since the compression surface is in a pressure gradient, as the suction behind the compression surface is reduced, high-pressure air will enter the downstream slots and exit through the upstream slots. Another factor contributing to these differences resulted from leakage behind the compression surface. For the tests previous to cutting the slots and grooves on the back of the compression surface, the metal-to-metal contact between the back of the compression surface and the duct was close enough to prevent an appreciable amount of leakage from the high-pressure to the low-pressure regions. After the grooves were cut, however, with little or no suction behind the compression surface, high-pressure air downstream could leak into the grooves and escape into the low-pressure regions upstream. Thus, even with the bleed slots closed, the no-compression-surface-slot tests could not be duplicated. Shown in figure 15 are data for a test with the slots closed, but suction was used

to bleed air around the edges of the compression surface. The pressure recovery was as high (0.90) as the other bleed configurations and dropped off in pressure recovery as the bleed-mass-flow ratio was reduced below 0.045. Although the results of these tests show that compression-surface bleed on an inlet of this type is quite effective in improving the pressure recovery and that the bleed-slot configuration is apparently not at all critical, it does not give any exact minimum quantities of bleed mass flow necessary to achieve the improved pressure recovery.

Total pressure distributions at the compressor station for the inlet with compression-surface bleed are shown in figure 16. For the four slot configurations shown, all had about the same radial distortion as the corresponding inlet without compression-surface bleed; the circumferential distribution was quite good.

The shadowgraphs of inlet II-B with diverter suction and with and without compression-surface bleed are shown in figure 17. In neither case does the normal shock seem to be completely swallowed for super-critical operation as it was for diverter A with suction. Without compression-surface bleed, for critical operation, the second shock wave, caused by the front of the compression surface, seems to have moved forward with increased back pressure. This suggests that the flow on the compression surface was tending to separate, which does not appear to be the case with compression-surface bleed since the second shock wave appeared independent of back pressure in the duct.

Performance of Inlet III-B

The performance of inlet III-B is presented in figure 18. This inlet was tested at Mach numbers of 1.76 and 1.60 in addition to 2.02 at which the previous configurations were tested. The effects of compression-surface position (measured as shown in fig. 3) and compression-surface bleed were investigated and the variation of pressure recovery and mass flow for the Mach number range was determined.

The results of the tests at $M_\infty = 2.02$ are shown in figure 18(a) with six compression-surface slots and figure 18(b) with four compression-surface slots. The critical pressure recovery was comparable with the best pressure recovery of inlet II-B. The subcritical stability, however, was substantially greater for inlet III-B. The subcritical stability range with six slots was about twice that for four slots. The effect of compression-surface position or compression-surface bleed-slot configurations on the mass-flow ratio was quite small; the maximum mass-flow ratio of inlet III-B was less than that of inlet II-B with either six or four compression-surface slots. Total-pressure distributions of inlet III-B, figures 19(a) and 19(b), follow the pattern of inlet II-A and show very little effect of compression-surface position or bleed-slot configurations.

The results of the tests at $M_\infty = 1.76$ are presented in fig-
ure 18(c) with four compression-surface slots and in figure 18(d) with
no compression-surface slots. With four compression-surface slots the
critical pressure recovery, maximum mass-flow ratio, and stable sub-
critical mass-flow range were very little changed from the $M_\infty = 2.02$
tests. With no compression-surface slots the mass-flow ratio decreased
measurably as the compression surface was move forward. The total-
pressure distributions, figures 19(c) and 19(d), show very little effect
of compression-surface position or compression-surface bleed; the decrease
in free-stream Mach number, however, did increase the distortion.

The results of the tests at $M_\infty = 1.60$ are presented in fig-
ure 18(e). With four compression-surface slots, the performance was
unaffected by compression-surface position. The maximum pressure recovery
was 0.91, a value 0.03 higher than the maximum pressure recovery of the
$M_\infty = 2.02$ and 1.76 tests, and barely exceeded the normal shock recovery.
With no compression-surface slots, the peak pressure-recovery value at
$M_\infty = 1.60$ was reduced slightly. The compression-surface position of
1.1 inches was tested without bleed to find the effect of failure of the
compression surface to move rearward from the $M_\infty = 2$ design position
upon deceleration to lower speeds. The entire curve was shifted to the
left and upwards slightly; the peak pressure recovery increased to about
0.93 and the maximum entering-mass-flow ratio decreased about 0.25 from
the design position for $M_\infty = 1.60$. The flow was quite steady despite
the large quantity of air being spilled. The total-pressure distributions
shown in figures 19(e) and 19(f) show very little change from the
$M_\infty = 1.76$ tests, the distortion remaining approximately the same.

Shadowgraphs of the inlet III-B tests are presented in figure 20.
These shadowgraphs of tests with four compression-surface slots were
typical of the shock-wave configurations for each Mach number. The normal
shock seemed to have been swallowed at minimum back pressure in all cases
shown.

Tests of Buzz Suppressors

Tests of inlet II-B at $M_\infty = 2.02$ and inlet III-B at $M_\infty = 1.76$
were made with the buzz suppressors installed as shown in figure 4(f).
These were designed to extend into the airstream in case of failure of
the bypass-door control mechanism and thus to stabilize the normal-shock
position to prevent severe buzz until the airplane can be decelerated to
some speed at which the inlet will not buzz. Preliminary tests at
$M_\infty = 2.02$ were made without the perforations, but the flow ahead of the
inlet was unsteady at all operating conditions; this unsteadiness was
eliminated, however, by perforating the buzz suppressors. At $M_\infty = 1.76$
the flow was steady with and without perforations, but since the perfora-
tions would be required at the higher Mach number, data are presented for
the perforated configuration

Data at $M_\infty = 2.02$ for inlet II-B and at $M_\infty = 1.76$ for inlet III-B are shown in figure 21. Included is a line of constant corrected air flow, passing through the $h = 0$ curve at an assumed operating point. If the buzz suppressors are extended the operating point will become the inter-section of the data curve, corresponding to the value of h to which they are extended. Thus, at $M_\infty = 2.02$, if the buzz suppressors are fully extended ($h = 0.9$ inch), the equilibrium pressure recovery and mass-flow ratio are 0.54 and 0.60, respectively. Intermediate values of h were tested at $M_\infty = 2.02$ to determine the feasibility of extending the buzz suppressors in a more gradual manner to eliminate such a large sudden change in mass flow and pressure recovery. Values of h below 0.5 inch resulted in a decrease in pressure recovery, but the decrease in mass-flow ratio was insufficient to intersect the con-stant corrected weight-flow curve. At values of h between 0.5 inch and 0.8 inch, the amount of subcritical stability was not proportional to the height of the buzz suppressors.

Total-pressure distributions of several values of h for the $M_\infty = 2.02$ tests and for $h = 0.9$ inch at $M_\infty = 1.76$ are shown in figure 22. The amount of distortion was not excessive. This was to be expected of an inlet operating at such low pressure recovery and mass-flow ratios. The contours were taken from the test point closest to the line of constant corrected air flow of figure 21. As the mass-flow ratio was decreased below these points, the pressure distribution improved rapidly, due to decreased velocity through the duct. The total-pressure profiles shown, therefore, represent the worst conditions at which the inlet would be required to operate.

Shadowgraphs of the flow with the buzz suppressors are shown in fig-ure 23. A normal shock wave stands ahead of the buzz suppressors at all operating conditions. With $h = 0.9$ inch at both $M_\infty = 1.76$ and 2.02, the normal shock is moved forward with increasing back pressure; whereas, with $h = 0.6$ inch at $M_\infty = 2.02$, the shock is not noticeably displaced. Thus, with $h = 0.9$ inch the amount of spillage possible before the normal shock becomes unstable is greater than for $h = 0.6$ inch and it was only with the buzz suppressors fully extended ($h = 0.9$) that movement of the normal shock permitted a large amount of spillage.

Tests of Rearward-Facing Control Tubes

The results of the tests of the rearward-facing control tubes located on the inboard wall of the duct are presented in figure 24. Details of these tubes and their locations are shown in figure 4(g). The control tubes were tested with inlet II-B at $M_\infty = 2.02$ with seven compression-surface slots, and with inlet III-B at $M_\infty = 2.02$, 1.76, and 1.60 with

four compression-surface slots. At $M_\infty = 2.02$ the control pressure at all points in both inlets increased abruptly as the normal shock wave moved forward and continued to increase with decreasing corrected air flow. The pressure variation of each tube with changing corrected air flow was considered adequate to provide a control signal to a bypass-door mechanism. For the $M_\infty = 1.76$ and 1.60 tests with inlet III-B, the curves became flatter near the minimum corrected air-flow points and the tubes did not respond individually. Thus, the problem of using the rearward-facing control tubes to indicate the normal-shock position or to provide a signal for control of bypass doors becomes more difficult as the free-stream Mach number is decreased. This did not seem to be associated with the farther-downstream locations of the control tubes, since the characteristics of all tubes were similar for the lower free-stream Mach numbers. The presence of the control tubes in the duct had no noticeable effect on pressure recovery, mass-flow ratio, or total-pressure distribution.

SUMMARY OF RESULTS

An experimental investigation of the performance of a 1/10-scale semielliptical scoop inlet designed for Mach number 2.0 was conducted in a jet facility of the Langley gas dynamics laboratory. Tests were made at Mach numbers of 2.02, 1.76, and 1.60, and Reynolds numbers of 2.05, 2.14, and 2.26×10^6 per inch, respectively. The effect of boundary-layer bleed, leading-edge configuration, the performance of a device to extend the subcritical stability of the inlet, and characteristics of rearward-facing control tubes near the inlet throat were investigated. The following results were obtained:

1. An increase of pressure recovery from 0.83 to 0.90 at a Mach number of 2.02 was obtained by use of boundary-layer bleed on the diverter and compression surface near the inlet throat. An increase in critical mass-flow ratio of 0.05 and improvement of the circumferential total-pressure distribution also resulted.

2. Improved starting and increased pressure recovery resulted from cutting slots in the leading edge or otherwise relieving the leading edge near the diverter.

3. Generally, modifications to the inlet, which resulted in improved starting characteristics and higher pressure recovery, decreased the subcritical stability range.

4. Adequate diverter bleed could be provided by using a diverter which exhausted the bleed air to the free stream.

DECLASSIFIED

5. For the configuration tested at all three Mach numbers (2.02, 1.76, and 1.60), the pressure recovery, entering mass-flow ratio, and total-pressure distribution showed little effect of free-stream Mach number.

6. Satisfactory buzz suppression for emergency purposes was obtained by extending perforated plates into the airstream ahead of the inlet.

7. Tests at a Mach number of 2.02 of the rearward-facing control tubes near the inlet throat showed the normal shock position could be determined. The pressure variation of each tube with changing corrected weight flow was considered adequate to provide a control signal to a bypass door mechanism. At the lower Mach numbers, the shock position could not be precisely determined from the control tubes.

Langley Aeronautical Laboratory,
    National Advisory Committee for Aeronautics,
        Langley Field, Va., June 24, 1957.

REFERENCES

1. Comenzo, Raymond J., and Mackley, Ernest A.: Preliminary Investigation of a Rectangular Supersonic Scoop Inlet With Swept Sides Designed for Low Drag at a Mach Number of 2.7. NACA RM L52J02, 1952.

2. Evvard, John C., and Moslen, Stephen H.: Three-Dimensional Supersonic Nozzles and Inlets of Arbitrary Exit Cross Section. NACA TN 2688, 1952.
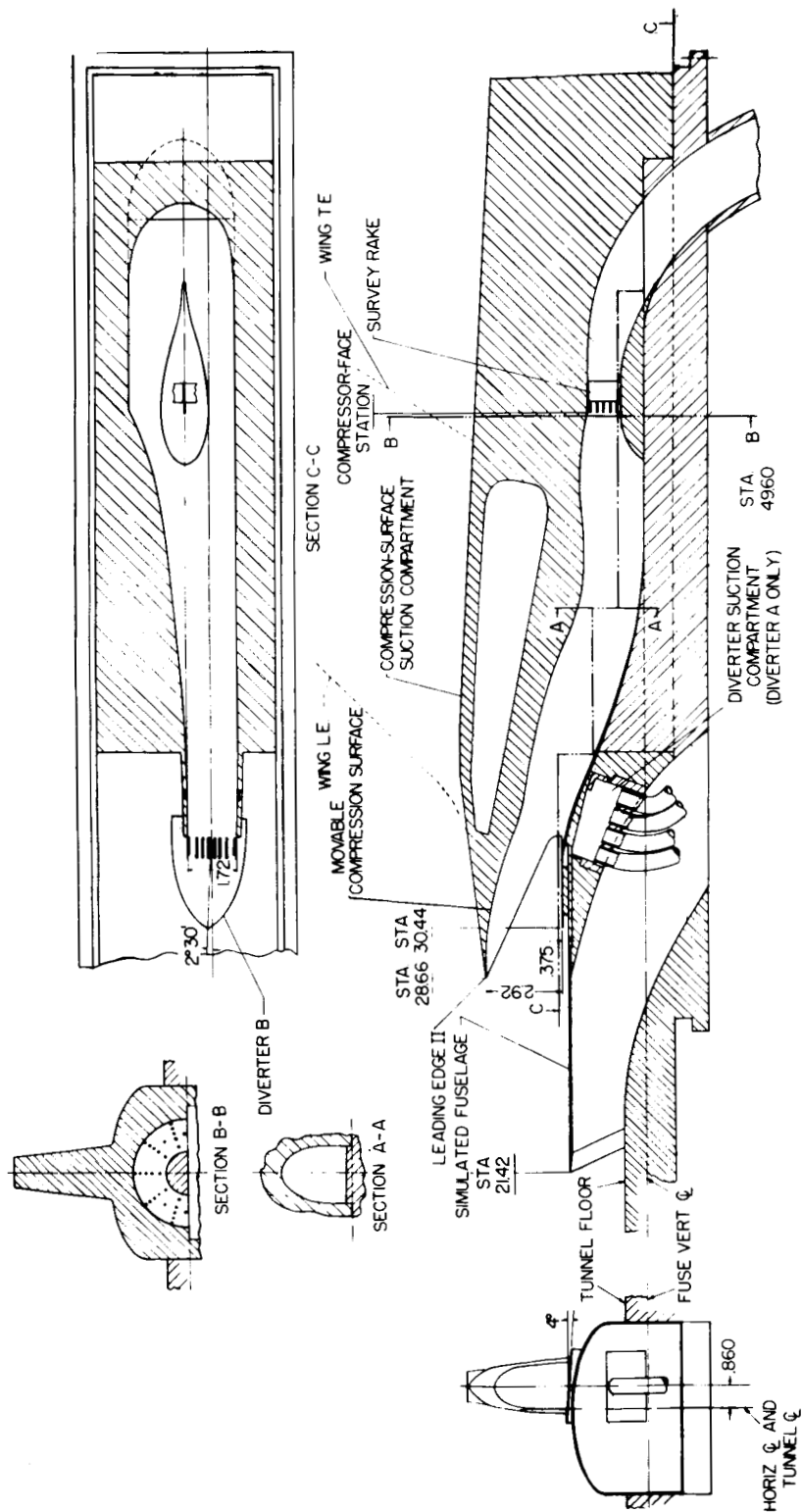
Figure 1.- Schematic drawing of model.
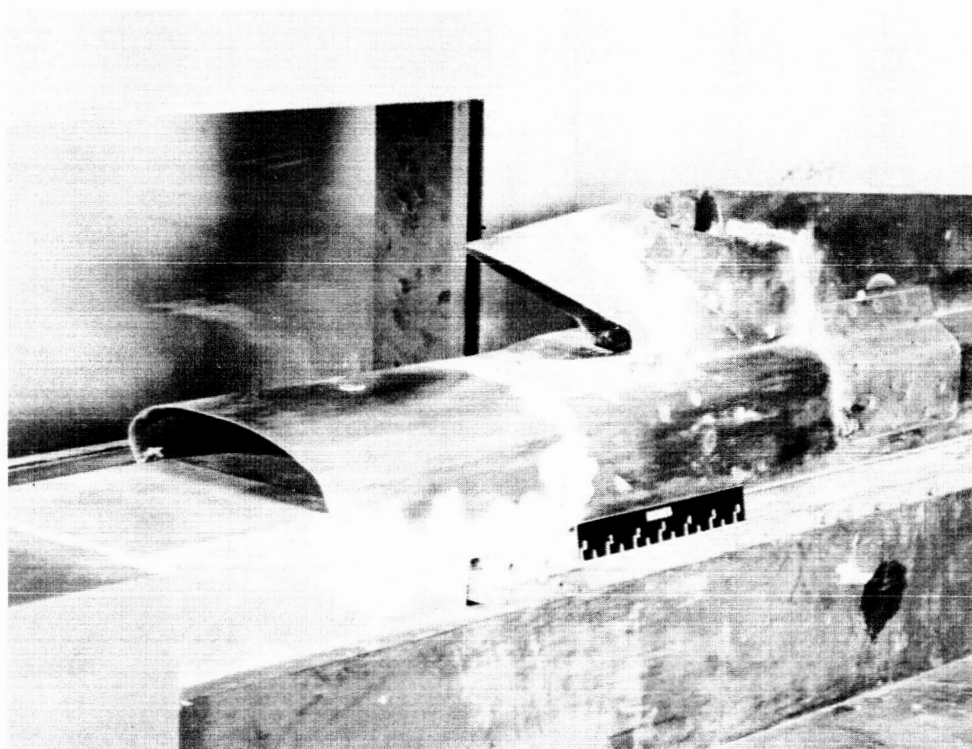
Figure 2.- Photograph of model.   L-57-212.1
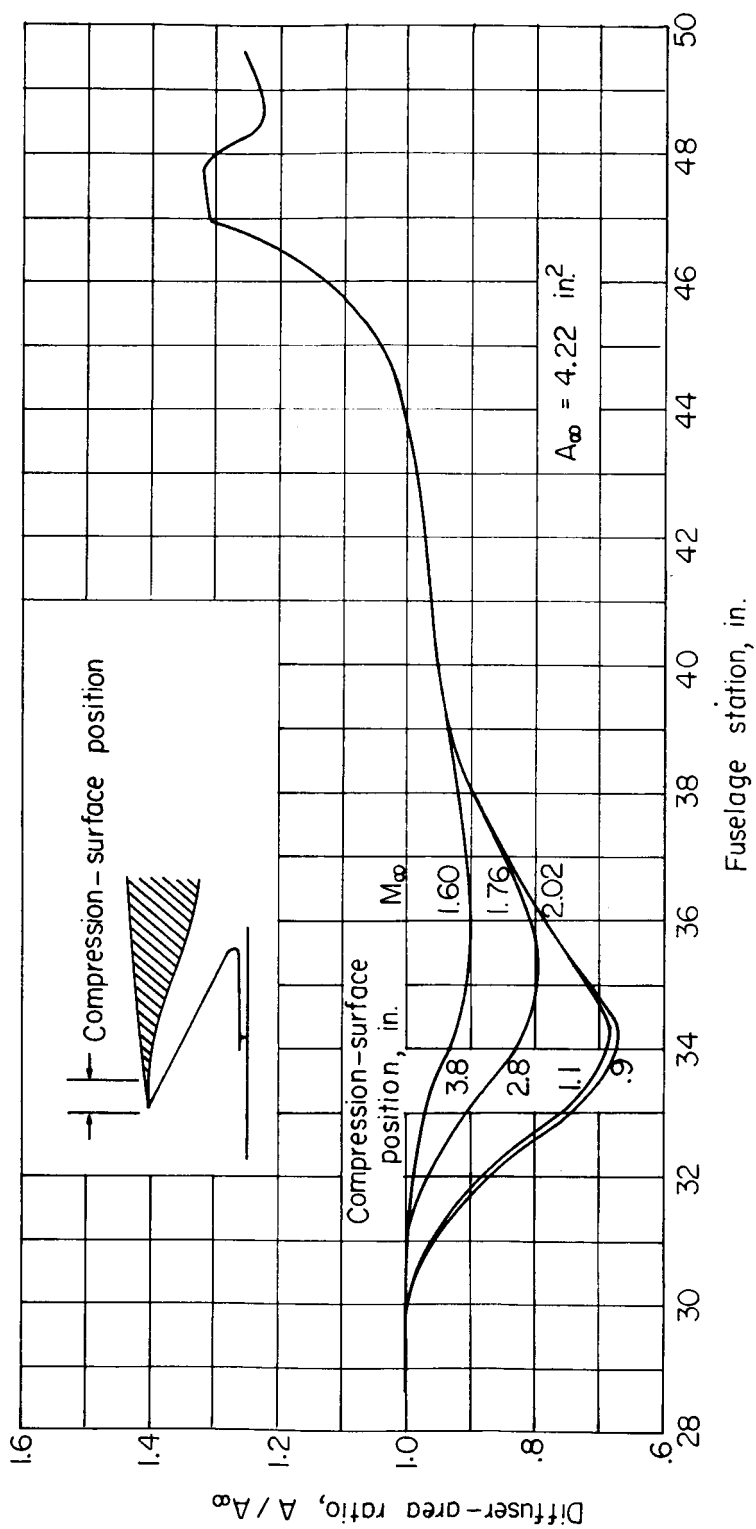
Figure 3.- Diffuser area variation.

Details of vertical slot
shown with side-wall slots
open (leading edge Ib)

.90   .80

.25

30°

Sta. 28.49

58°   A

A

.38

1.40

Side-wall slots
(leading edge Ia)

Leading edge I

2.92

4°

1.70

1.90

This view typical for
all three leading edges

5°

Section A-A

Sta. 28.87

65°   A

A

.75 R

5.45   .10

Leading edge II

60°
58°
.92

Sta. 28.49

65°

5.09
5.17
5.59
5.63

45°
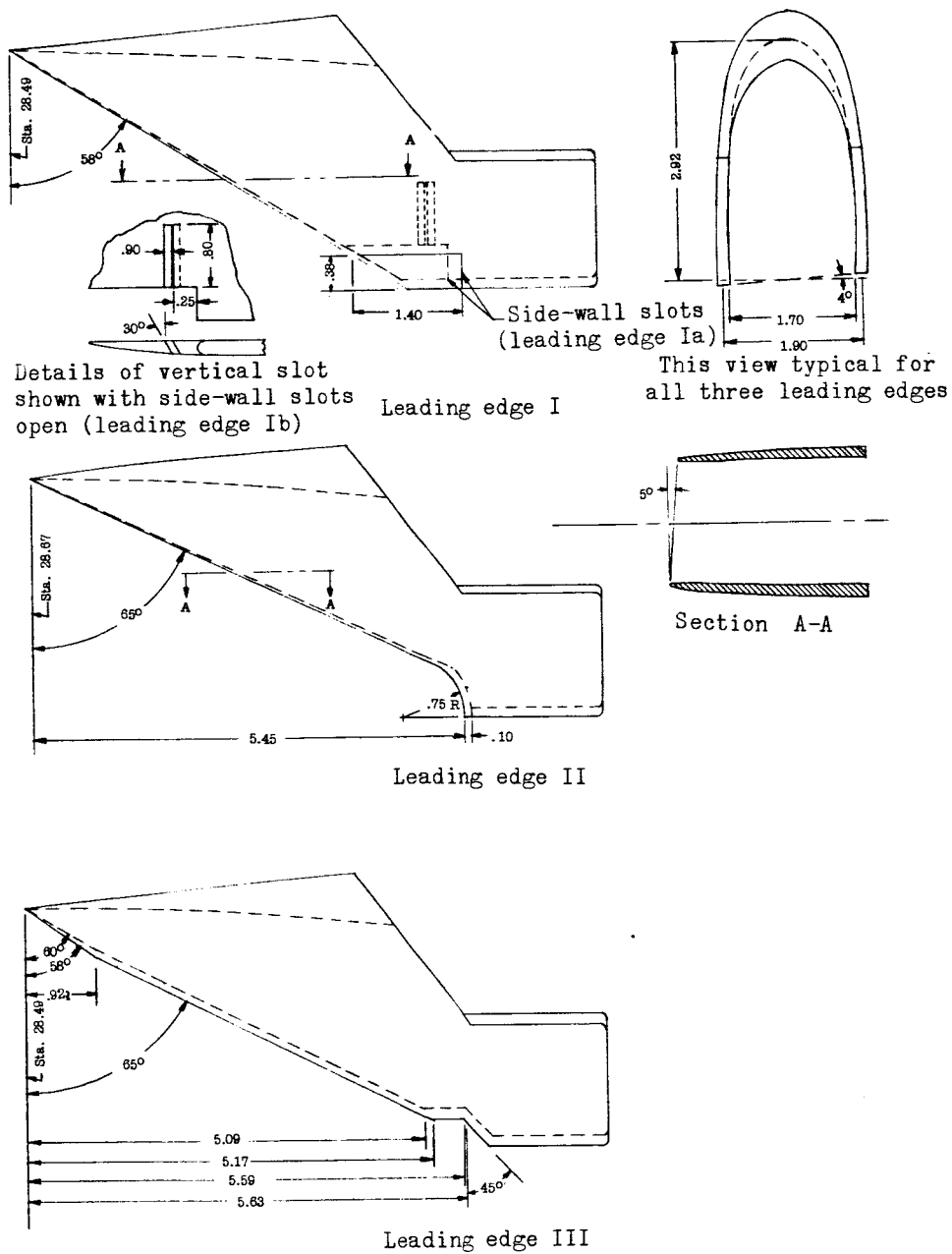
Leading edge III

(a) Leading edges.

Figure 4.- Details of model. (Dimensions are in inches.)
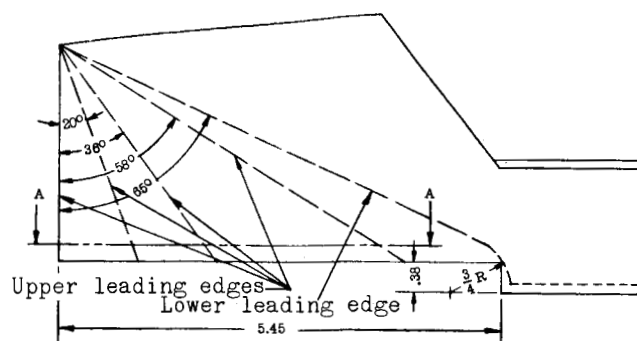
0°-65°, 20°-65°, 36°-65°, and 58°-65° leading edges
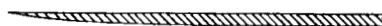
Section A-A
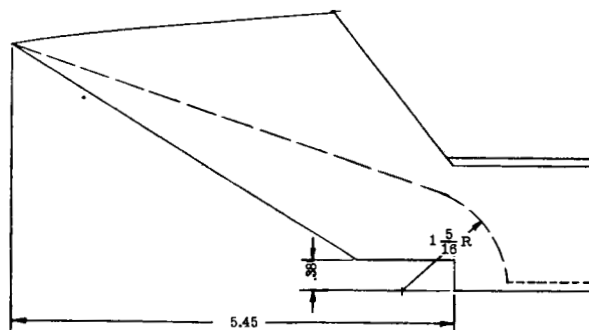
58°-71° leading edge

(b) Staggered leading edges.

Figure 4.- Continued.

Section A-A

Diverter A

Section A-A

Section B-B
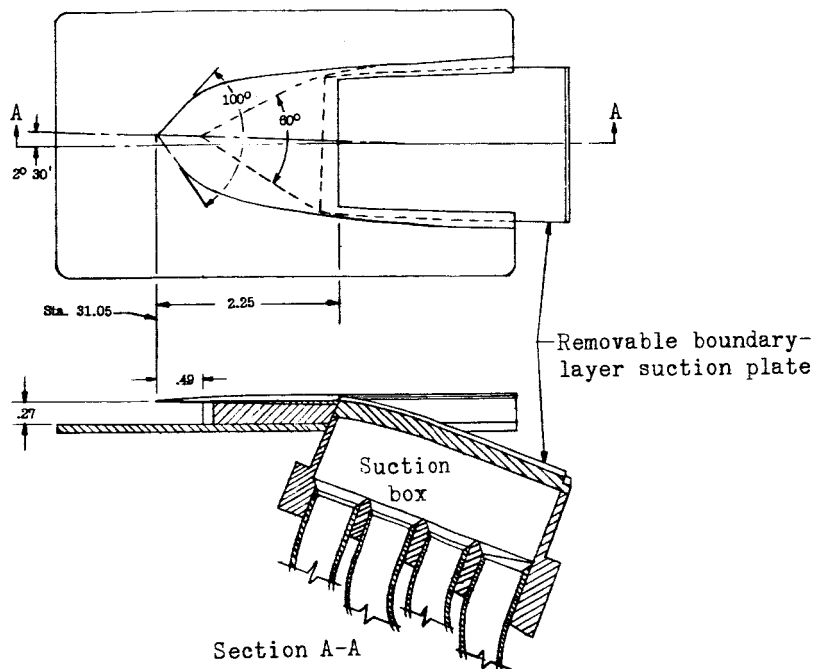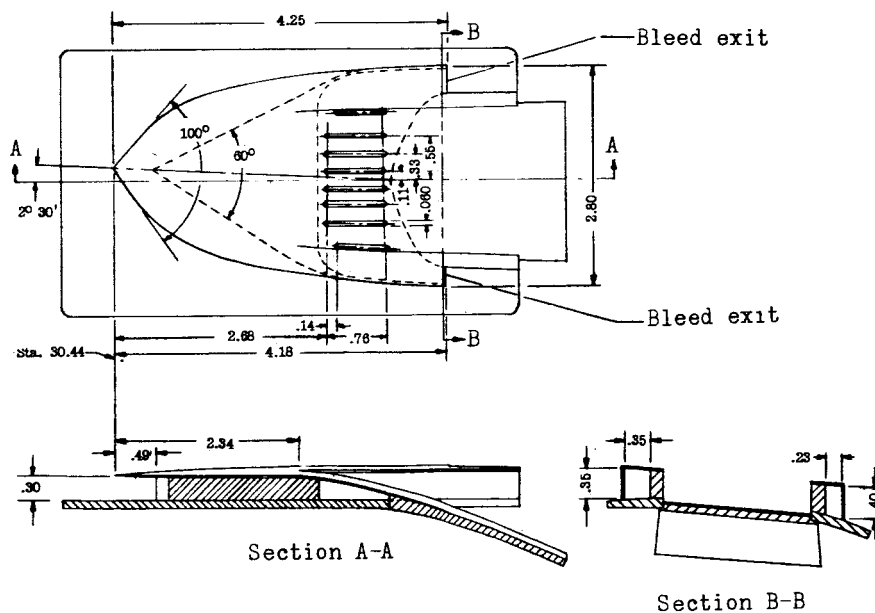
Diverter B

(c) Boundary-layer diverters.

Figure 4.- Continued.

.100

.40

Configuration 1

.07
.15
.22
.125

Configuration 5

.10
.50

Configuration 2

.25

Configuration 6

.10
.50
.125

Configuration 3

Removable boundary-
layer suction plate

.25
.85

Configuration 7

.60

Configuration 4

Note: All slots and holes are
swept back 45° from surface;
all slots except configuration 1
are 0.060 wide; all holes are
0.060 diameter
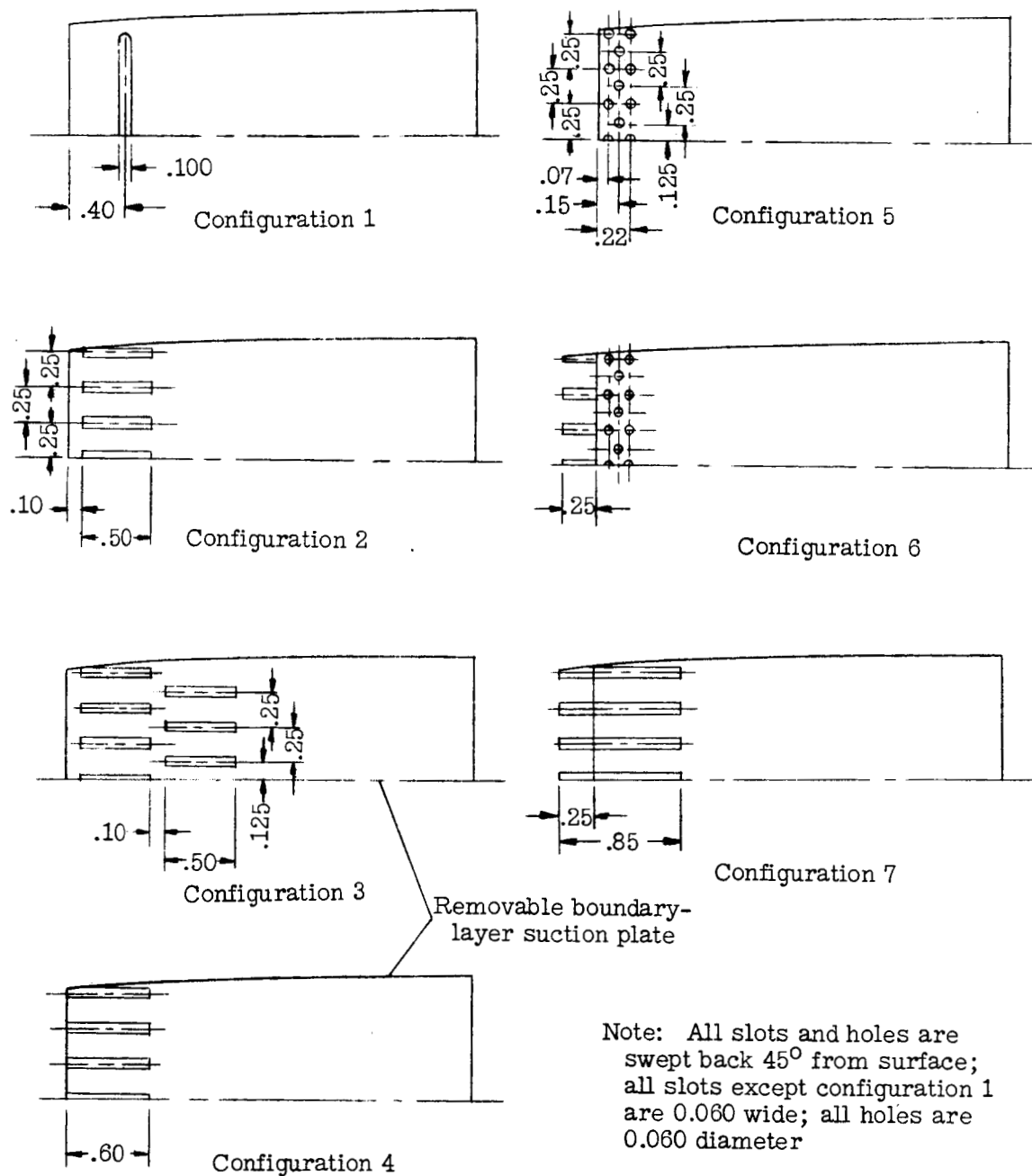
(d) Diverter A slot configurations.

Figure 4.- Continued.

Slots used for four-slot configuration

Note: All slots 0.060 wide

Grooves leading from slots
to suction compartment
are deepened at slots to
within 1/32 of compression
surface

.60

.40

.20

.50

.50

.50

.50

2.08

2.91

3.74

4.56
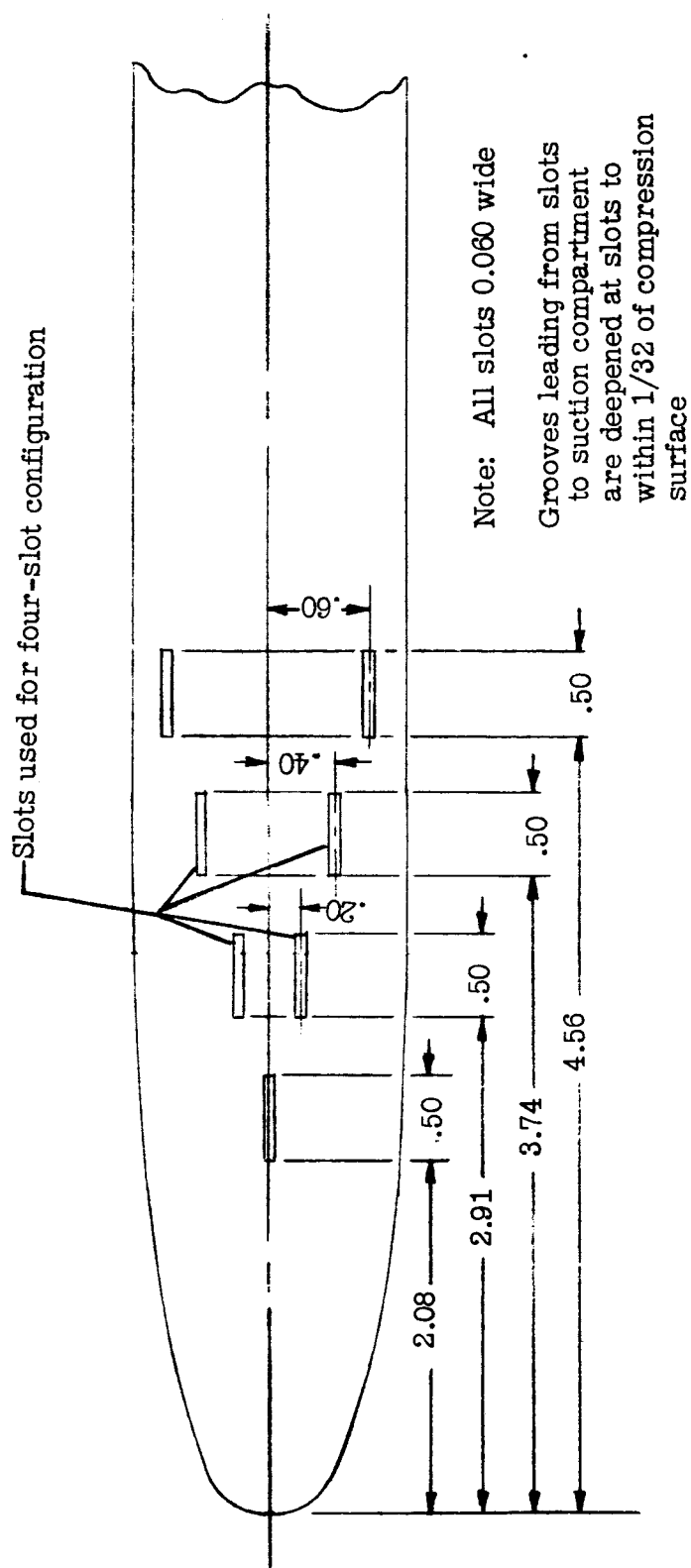
(e) Compression-surface suction slots.

Figure 4.- Continued.

2.08
2.24

.90

12°

12°

4°

.62

.62

1/16-diam. holes,
each approximately
evenly spaced

h

Pivot points

Partially retracted position
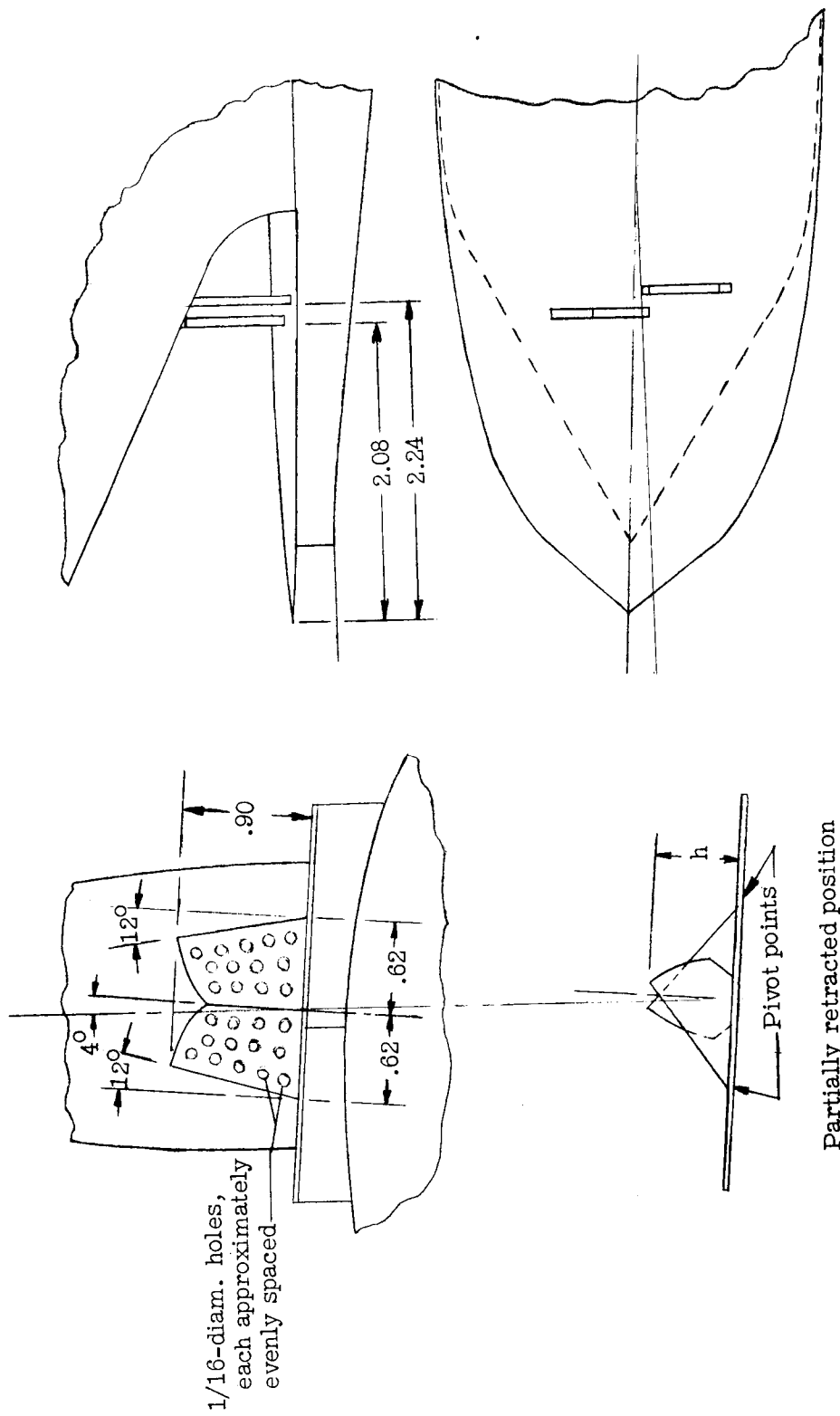
(f) Buzz suppressors.

Figure 4.- Continued.

All tubes spaced 0.350 center
to center measured along
inboard duct wall

$\frac{1}{4}$ duct height

$\frac{1}{8}$ duct height

$\frac{1}{4}$ duct height

Sta. 34.02

.125

.20

.060–.040 tube
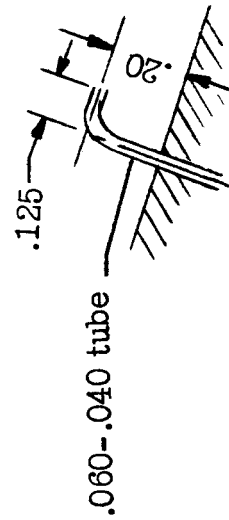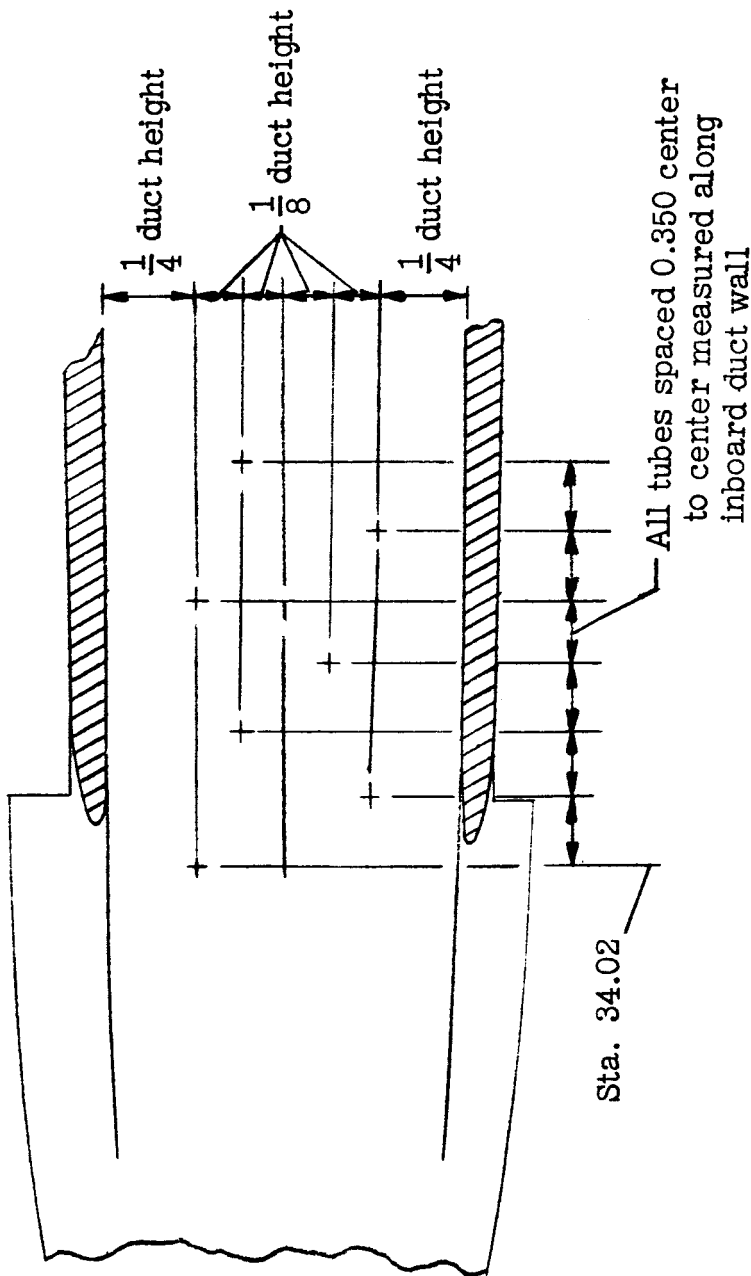
(g) Control tubes.

Figure 4.- Concluded.
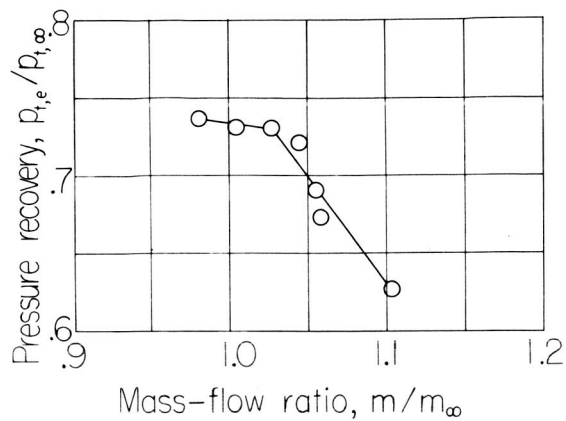
(a) Variation of pressure recovery
with mass-flow ratio
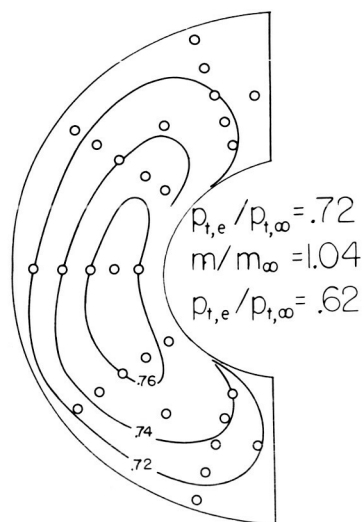
(b) Total-pressure distribution

$p_{t,e}/p_{t,\infty} = .72$
$m/m_{\infty} = 1.04$
$p_{t,e}/p_{t,\infty} = .62$
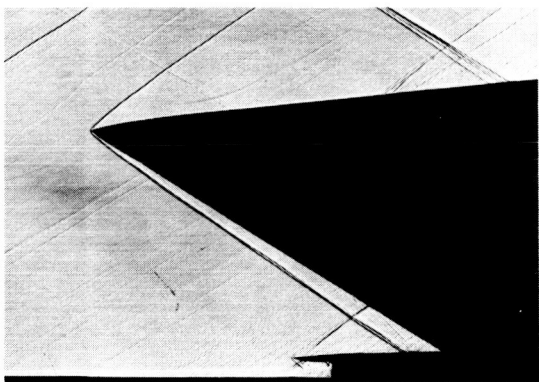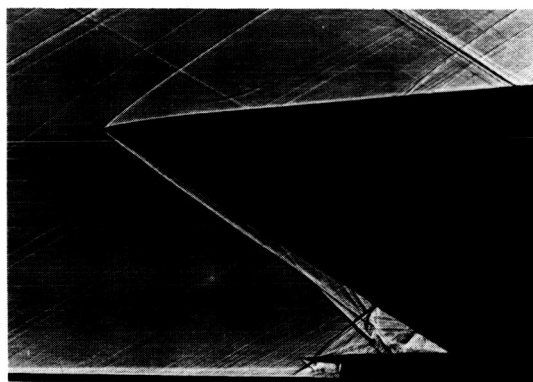
Supercritical   Critical

(c) Shadowgraphs

Figure 5.- Performance of inlet I-A. $M_{\infty} = 2.02$.   L-57-2700

UNCLASSIFIED
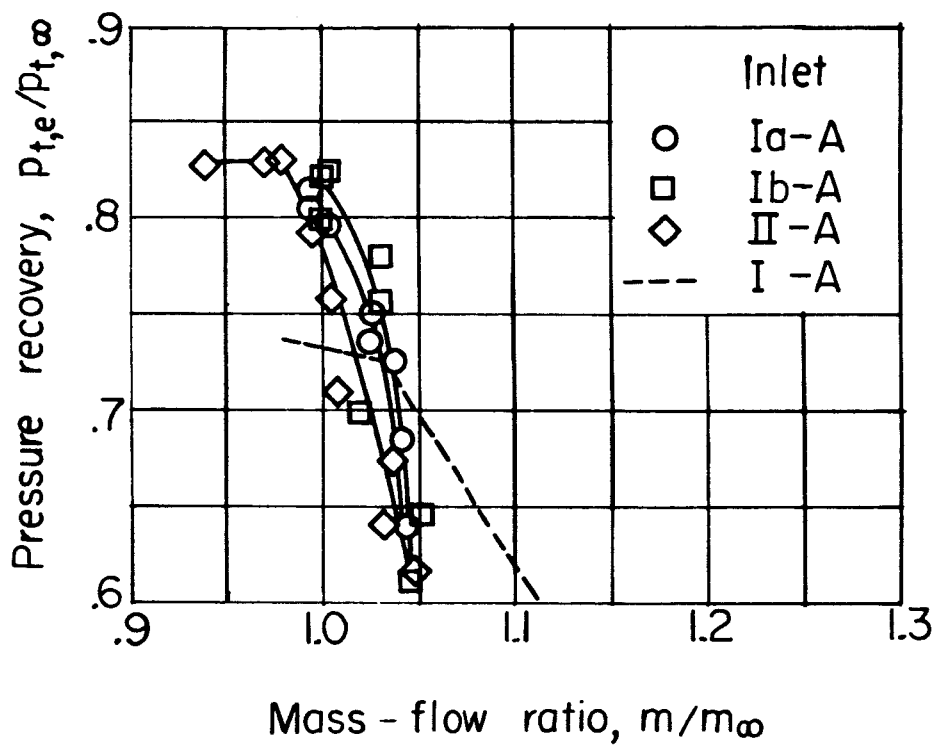
Figure 6.- Performance of inlets Ia-A, Ib-A, and II-A without diverter bleed. $M_\infty = 2.02$.

⠿⠿⠿⠿⠿⠿

$p_{t,e}/p_{t,\infty} = .72$

$m/m_\infty = 1.04$

$p/p_{t,\infty} = .62$

.76

.74

.72

Inlet I-A

.88

.86

.84

.82

.80

.78

$p_{t,e}/p_{t,\infty} = .81$

$m/m_\infty = .99$

$p/p_{t,\infty} = .69$

Inlet Ia-A

.88

.86

.84

.82

.80

.78

$p_{t,e}/p_{t,\infty} = .82$

$m/m_\infty = 1.00$

$p/p_{t,\infty} = .74$

Inlet Ib-A

$p_{t,e}/p_{t,\infty} = .83$

$m/m_\infty = .98$

$p/p_{t,\infty} = .69$

.88

.86

.84

.82

.80

.78
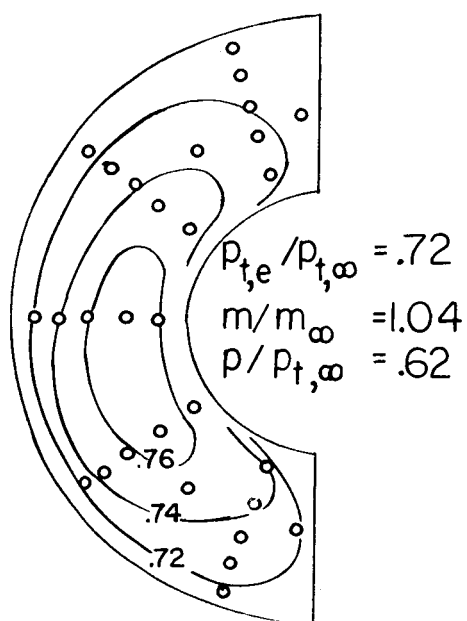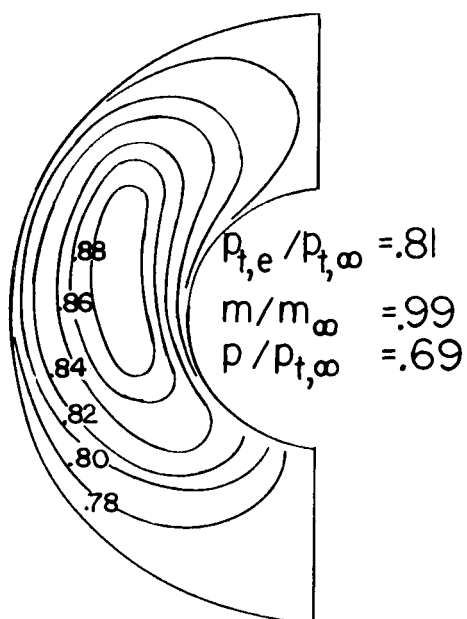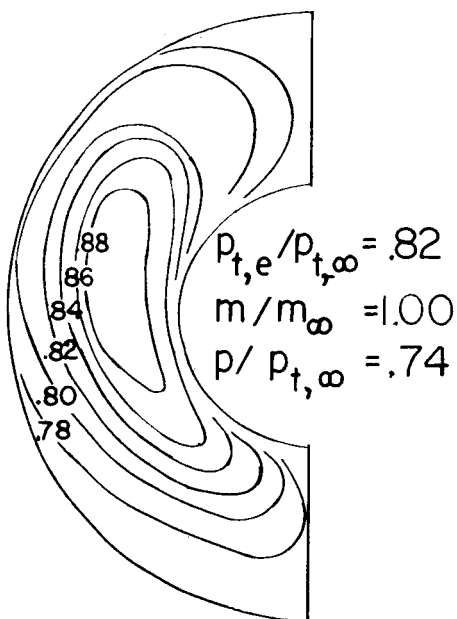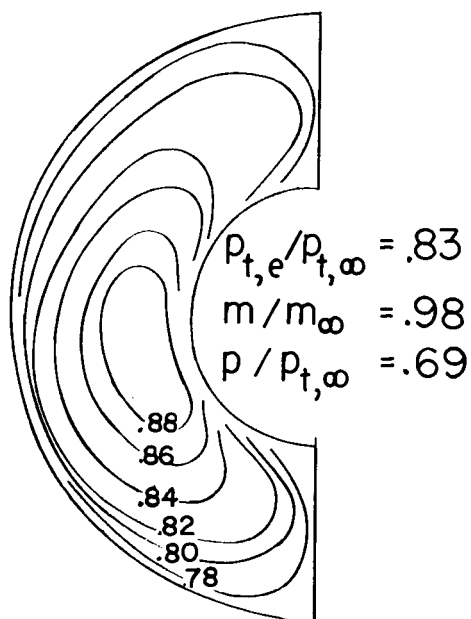
Inlet II-A

Figure 7.- Total-pressure distributions of inlets I-A, Ia-A, Ib-A, and II-A without diverter bleed. $M_\infty = 2.02$.
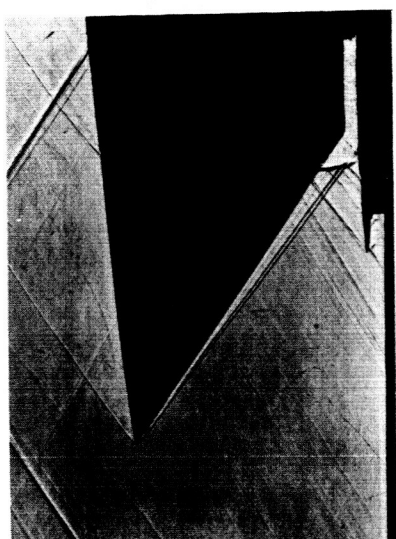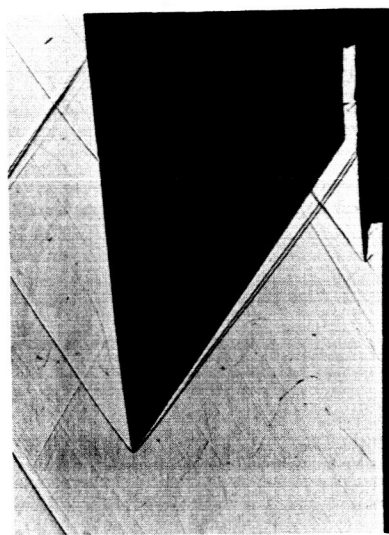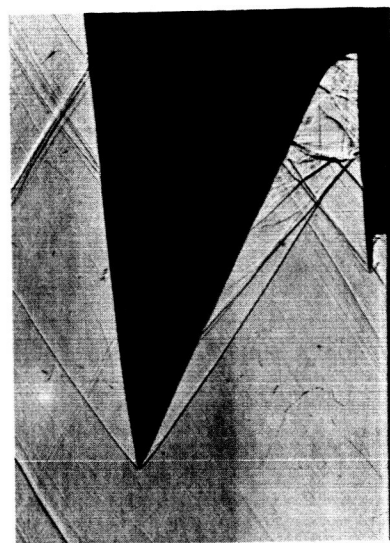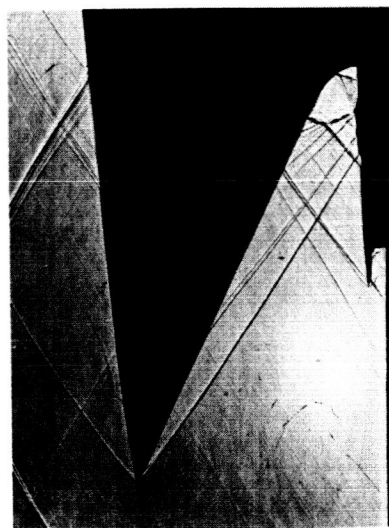
Figure 8.- Shadowgraphs of inlets Ia-A and II-A without diverter bleed. $M_\infty = 2.02$.

L-57-2701
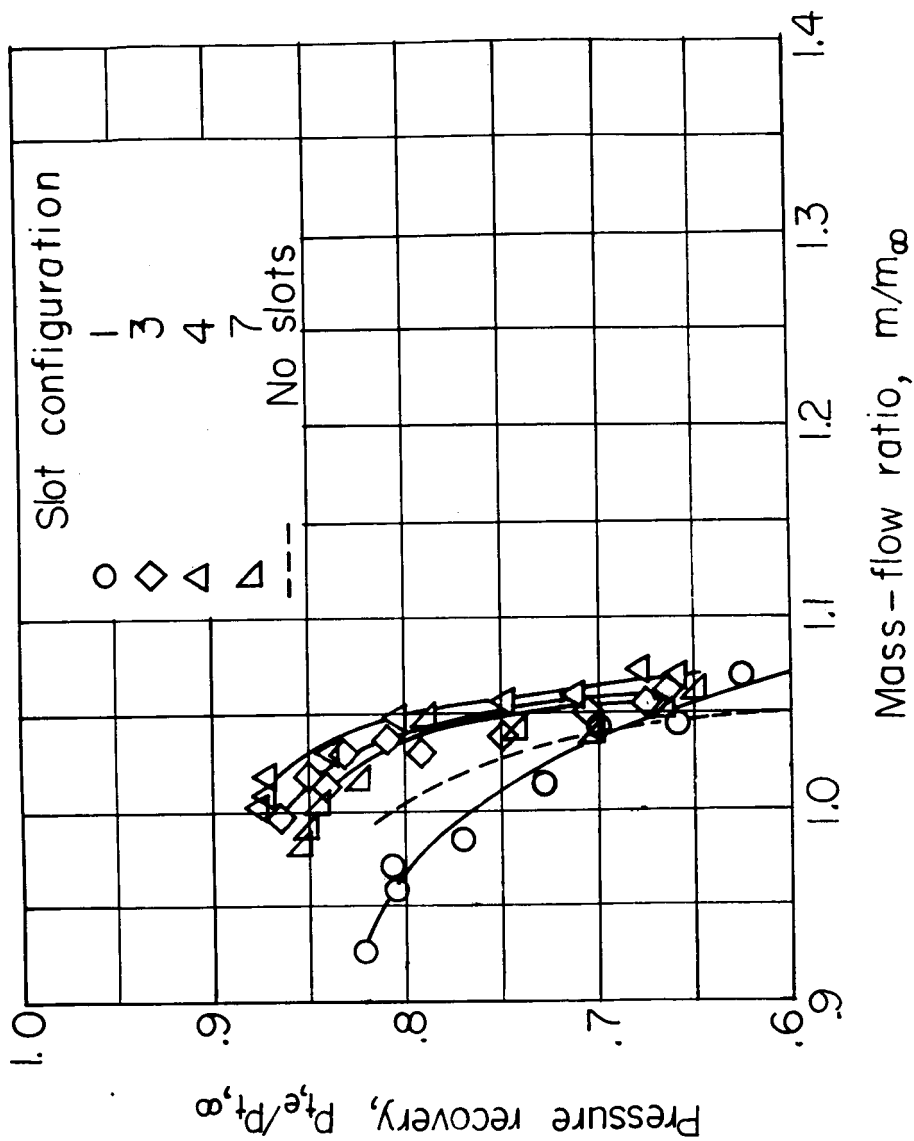
(a) Inlet Ia-A.

Figure 9.- Performance of several diverter boundary-layer slot configura-
tions. $M_\infty = 2.02$.
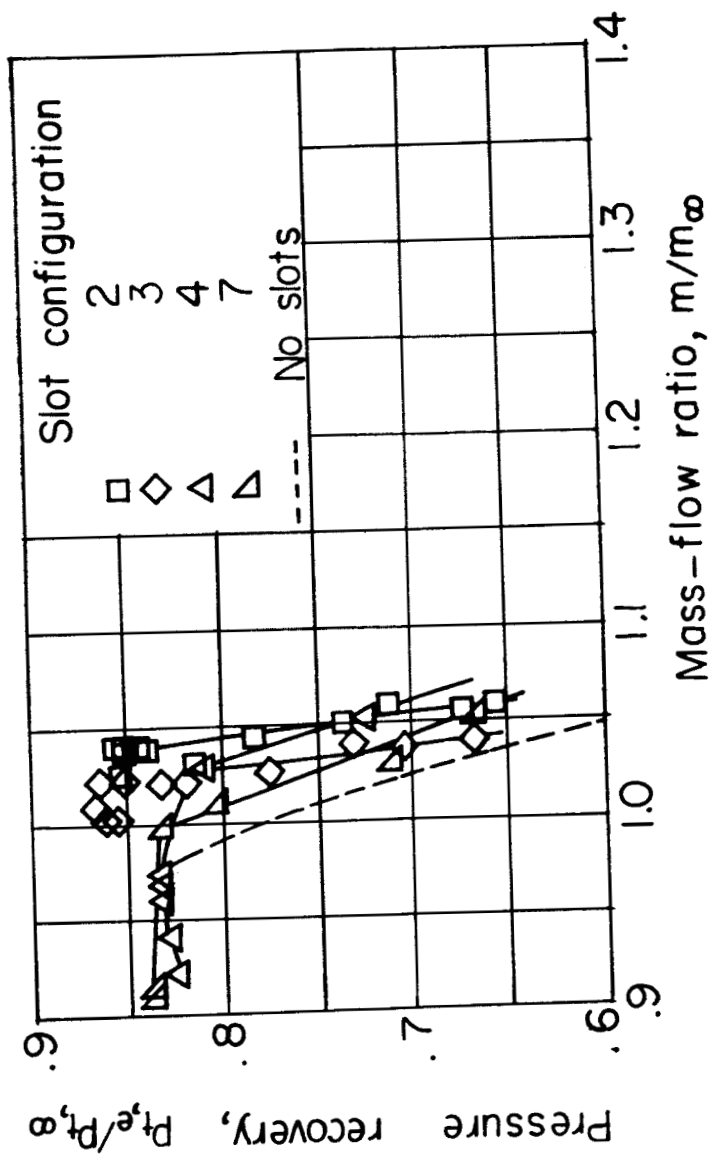
(b) Inlet II-A.

Figure 9.- Continued.
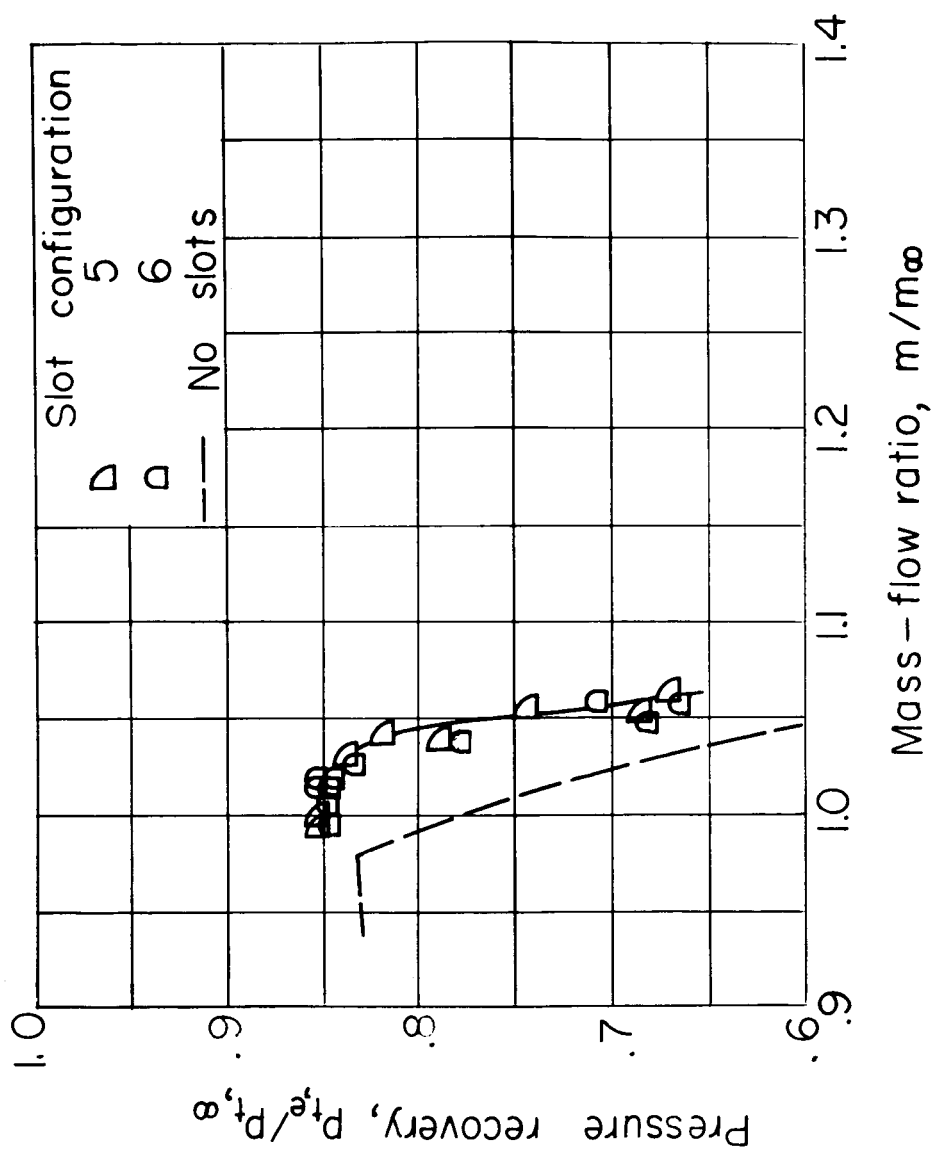
(c) Inlet II-A with holes.

Figure 9.- Concluded.
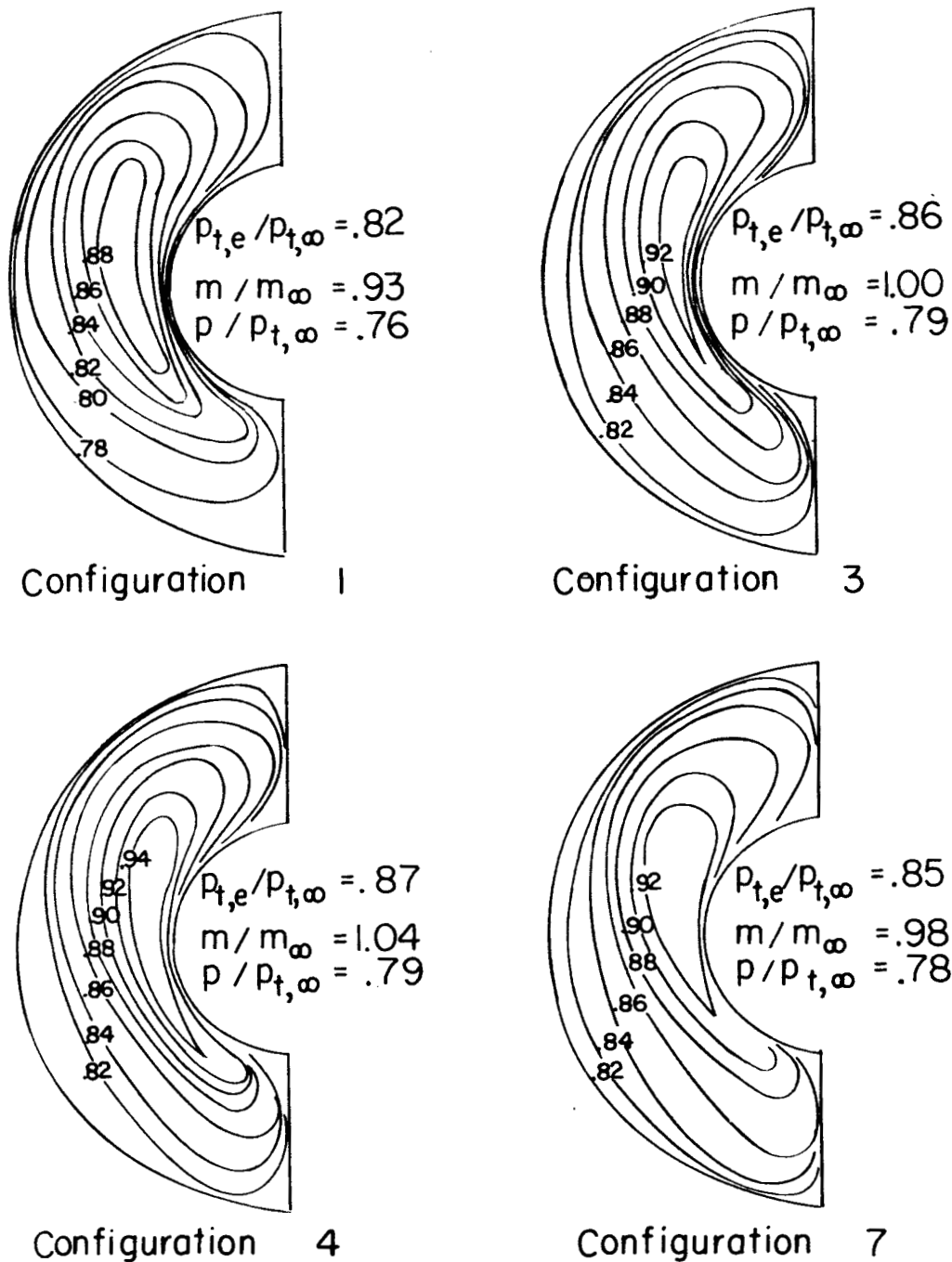
(a) Inlet Ia-A.

Figure 10.- Total-pressure distributions of inlets with several diverter boundary-layer slot configurations. $M_\infty = 2.02$.

$p_{t,e}/p_{t,\infty} = .86$

$m/m_\infty = 1.04$

$p/p_{t,\infty} = .78$

.92
.90
.88
.86
.84
.82
.80

Configuration 2

$p_{t,e}/p_{t,\infty} = .86$

$m/m_\infty = 1.01$

$p/p_{t,\infty} = .80$

.92
.90
.98
.96
.84
.82

Configuration 3

$p_{t,e}/p_{t,\infty} = .83$

$m/m_\infty = .96$

$p/p_{t,\infty} = .75$

.88
.86
.84
.82
.80

Configuration 4

$p_{t,e}/p_{t,\infty} = .83$

$m/m_\infty = 1.03$

$p/p_{t,\infty} = .74$

.88
.86
.84
.82
.80
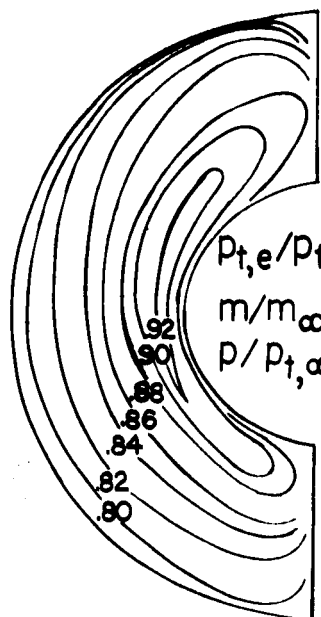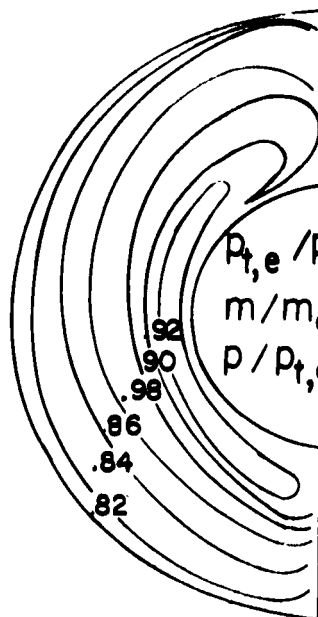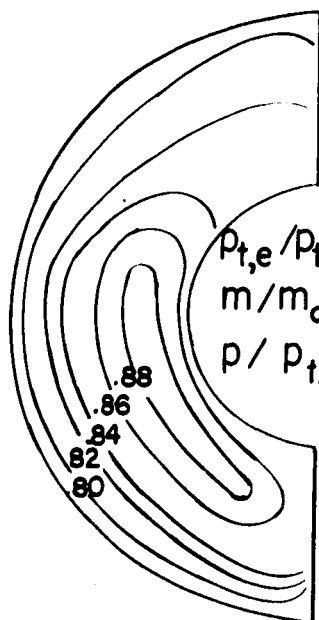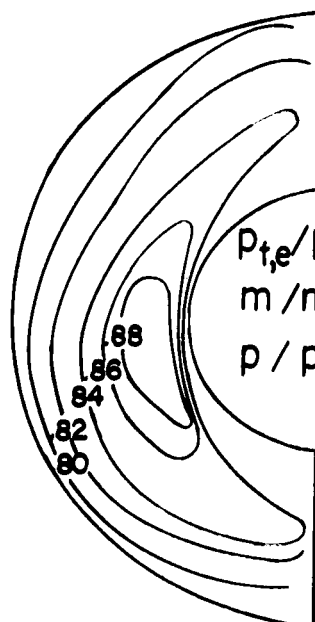
Configuration 7

(b) Inlet II-A.

Figure 10.- Continued.

$p_{t,e}/p_{t,\infty} = .85$
$m/m_\infty = .99$
$p/p_{t,\infty} = .76$

.90
.88
.86
.84
.82

Configuration   5

$p_{t,e}/p_{t,\infty} = .85$
$m/m_\infty = 1.02$
$p/p_{t,\infty} = .76$

.90
.88
.86
.84
.82
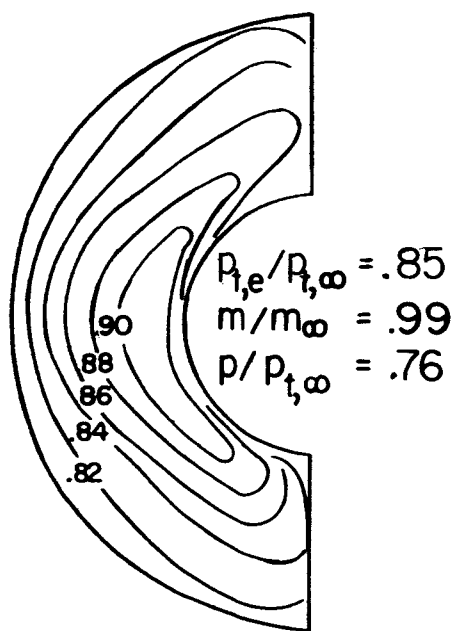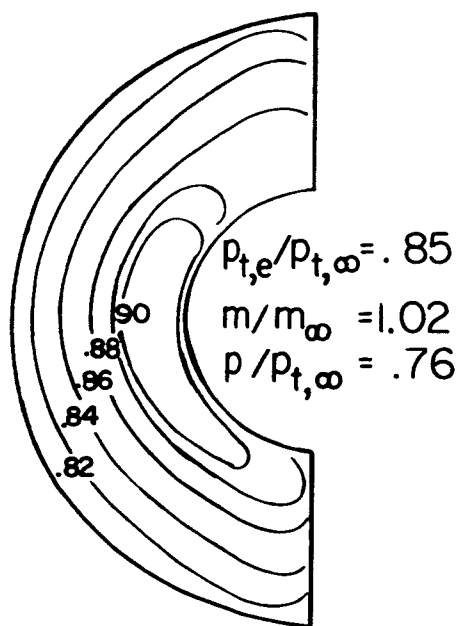
Configuration   6

(c) Inlet II-A with holes.

Figure 10.- Concluded.
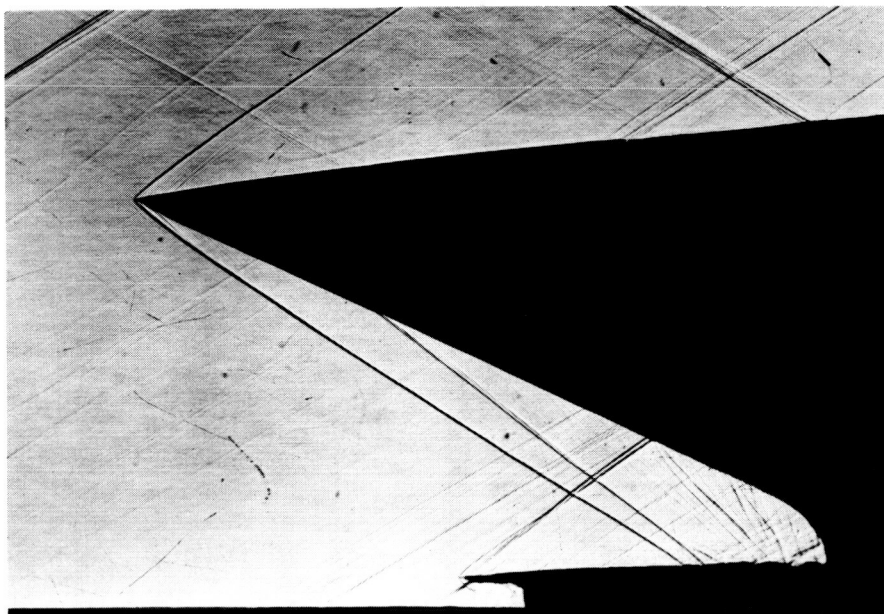
Supercritical operation
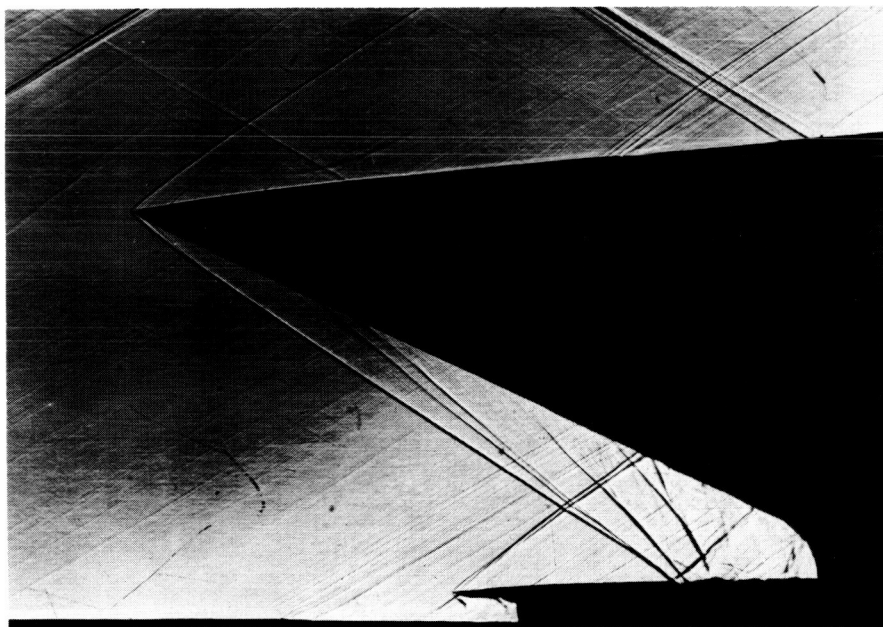
Critical operation

L-57-2702

Figure 11.- Shadowgraphs of inlet II-A with diverter boundary-layer slot configuration 7. $M_\infty = 2.02$.
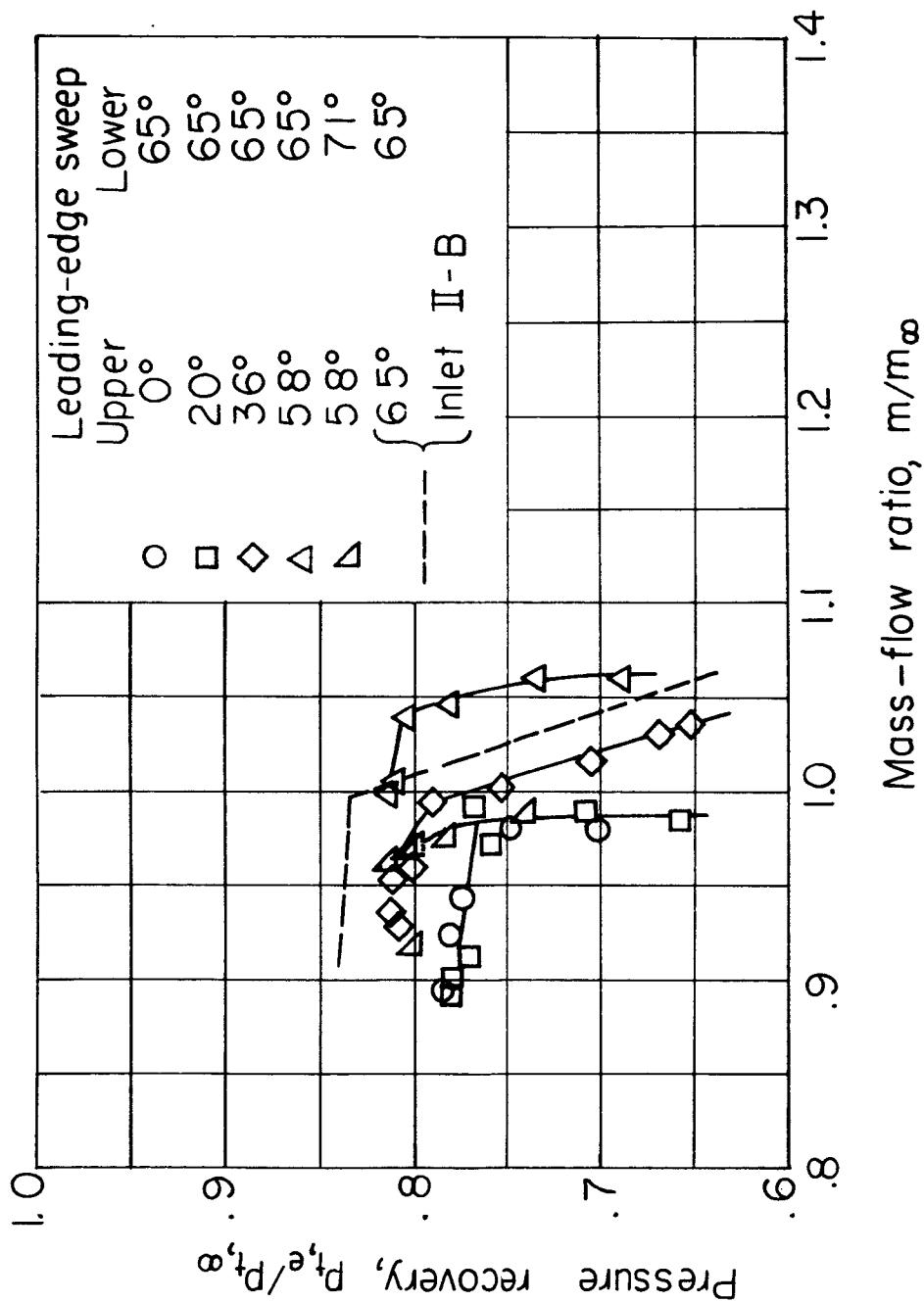
Figure 12.- Effect of inlet-leading-edge sweep angle on inlet pressure recovery and entering mass flow with diverter A and diverter boundary-layer slot configuration 7. $M_\infty = 2.02$.

$p_{t,e}/p_{t,\infty} = .77$

$m/m_\infty = .95$

$p/p_{t,\infty} = .68$

0° - 65°

$p_{t,e}/p_{t,\infty} = .78$

$m/m_\infty = .90$

$p/p_{t,\infty} = .70$

20° - 65°

$p_{t,e}/p_{t,\infty} = .80$

$m/m_\infty = .96$

$p/p_{t,\infty} = .71$

36° - 65°
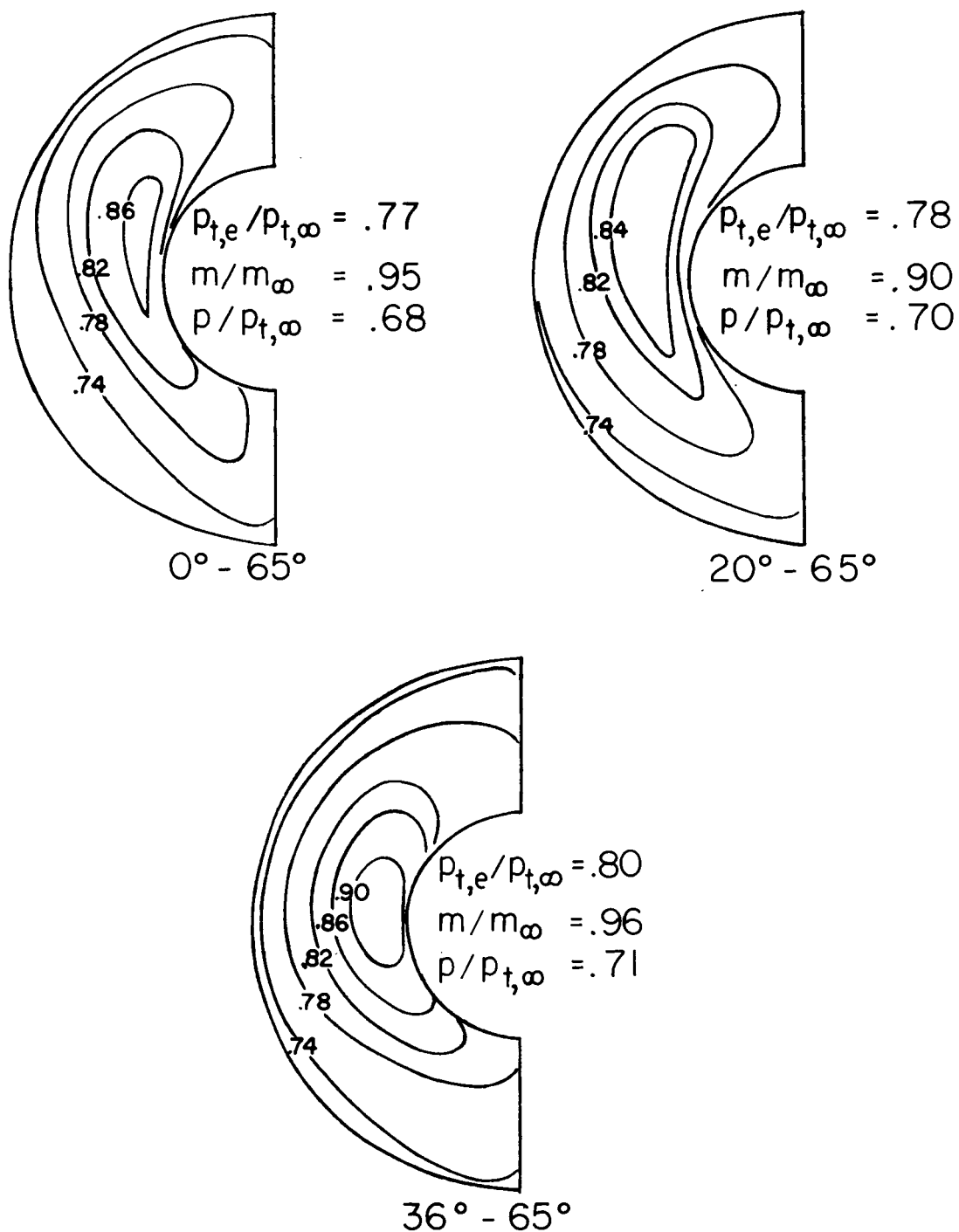
Figure 13.- Total-pressure distributions of inlet with various upper-
and lower-leading-edge sweep angles with diverter A and diverter
boundary-layer slot configuration 7. $M_\infty = 2.02$.

$$p_{t,e}/p_{t,\infty} = .81$$
$$m/m_{\infty} = 1.00$$
$$p/p_{t,\infty} = .73$$

.90
.86
.82
.78

58° - 65°

$$p_{t,e}/p_{t,\infty} = .81$$
$$m/m_{\infty} = .96$$
$$p/p_{t,\infty} = .73$$

.88
.86
.82
.78

58° - 71°
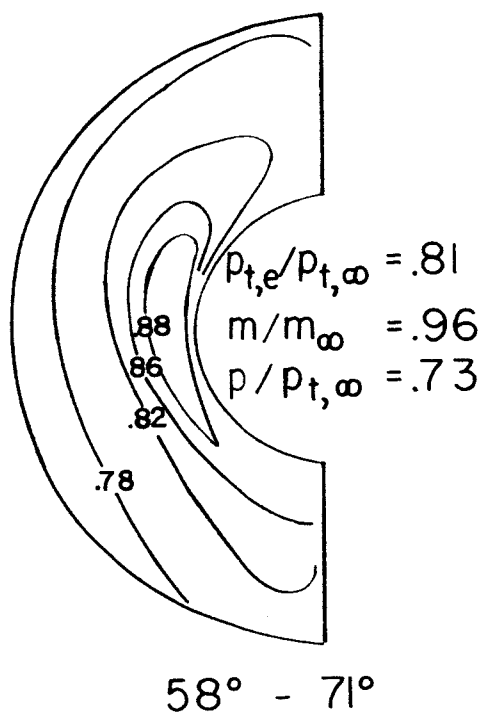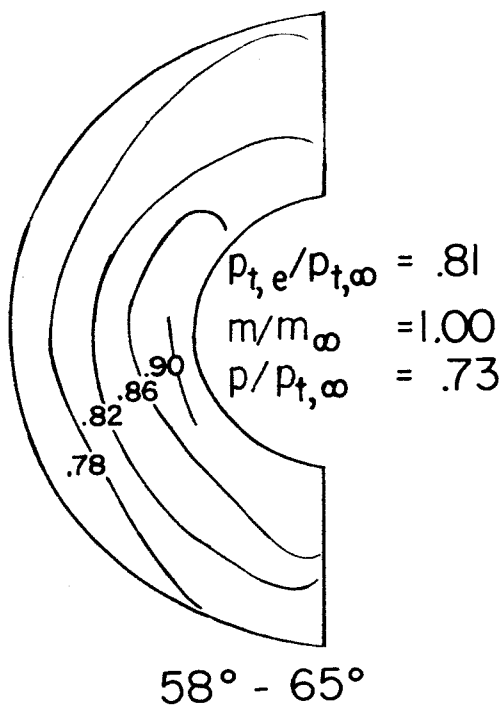
Figure 13.- Concluded.

Figure 14.- Effect of compression-surface bleed on pressure recovery and mass flow for inlet II-B with several bleed-slot configurations. $M_\infty = 2.02$.
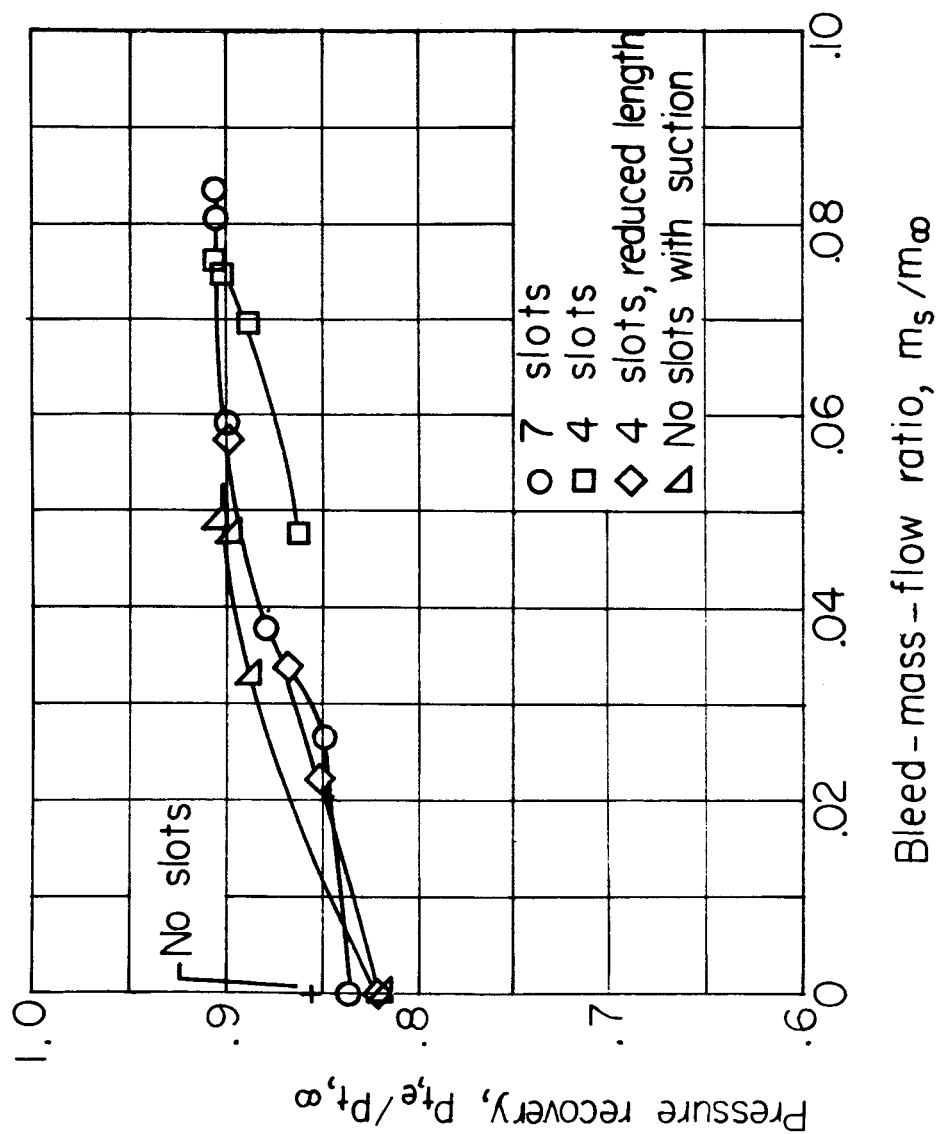
Figure 15.- Effect of compression-surface bleed mass flow on maximum pressure recovery for inlet II-B with several bleed-slot configurations. $M_\infty = 2.02$.
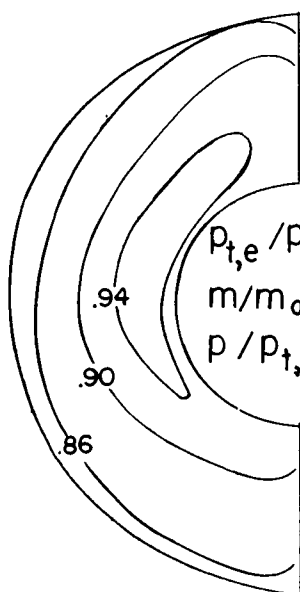
$$p_{t,e}/p_{t,\infty} = .90$$
$$m/m_\infty = 1.04$$
$$p/p_{t,\infty} = .81$$

.94
.90
.86

7 Compression-surface slots
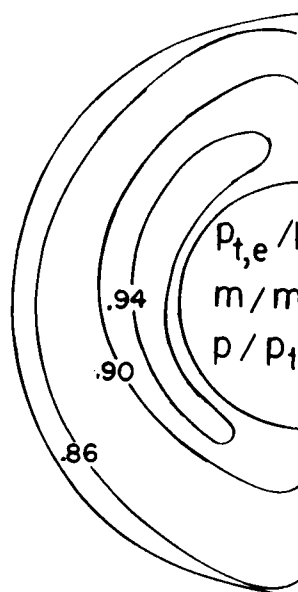
$$p_{t,e}/p_{t,\infty} = .90$$
$$m/m_\infty = 1.01$$
$$p/p_{t,\infty} = .81$$

.94
.90
.86

4 Compression-surface slots
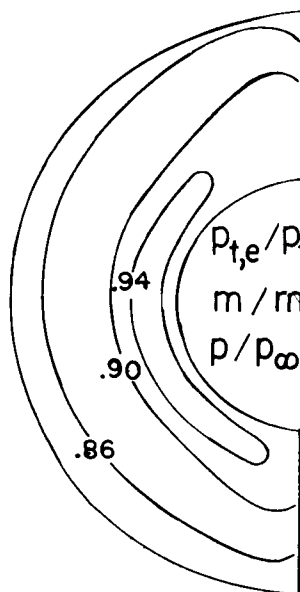
$$p_{t,e}/p_{t,\infty} = .90$$
$$m/m_\infty = 1.01$$
$$p/p_\infty = .81$$

.94
.90
.86

4 Compression-surface slots,
reduced length

Figure 16.- Total-pressure distributions of inlet II-B with several compression-surface-bleed slot configurations, and without compression-surface bleed. $M_\infty = 2.02$.

$$\frac{p_{t,e}}{p_{t,\infty}} = .86$$

$$\frac{m}{m_\infty} = .96$$

$$\frac{p}{p_{t,\infty}} = .78$$

.90

.86

.82
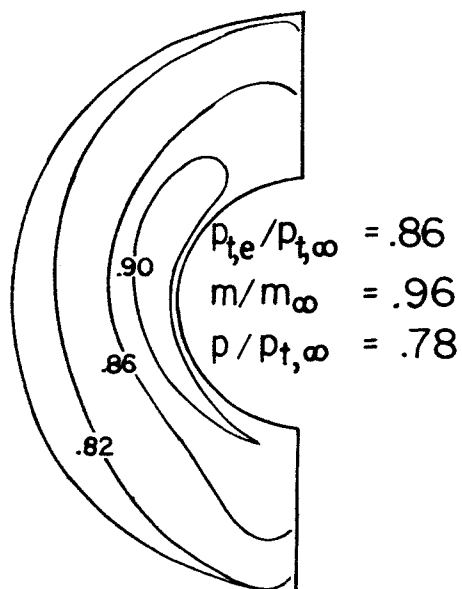
7 Compression-surface slots
No diverter slots

$$\frac{p_{t,e}}{p_{t,\infty}} = .86$$

$$\frac{m}{m_\infty} = .97$$

$$\frac{p}{p_{t,\infty}} = .77$$

.90

.88

.86

.84

.82
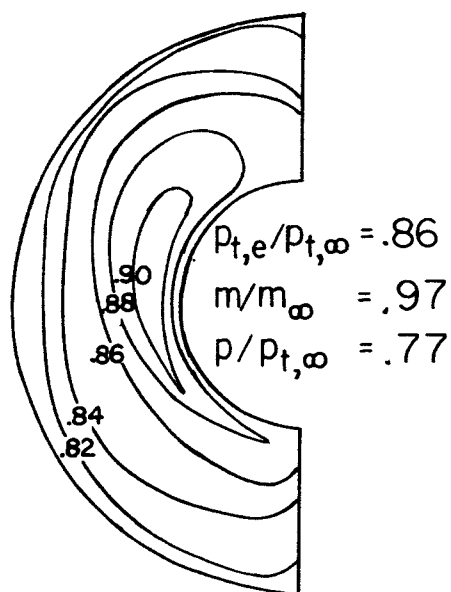
No compression-
surface bleed

Figure 16.- Concluded.
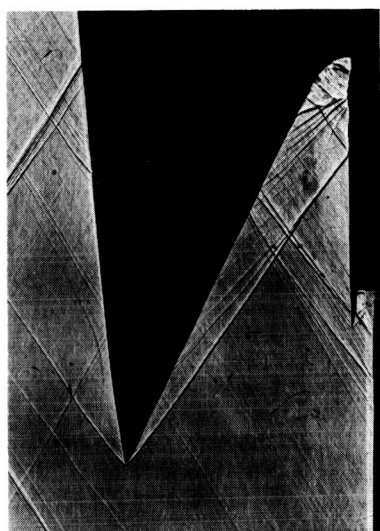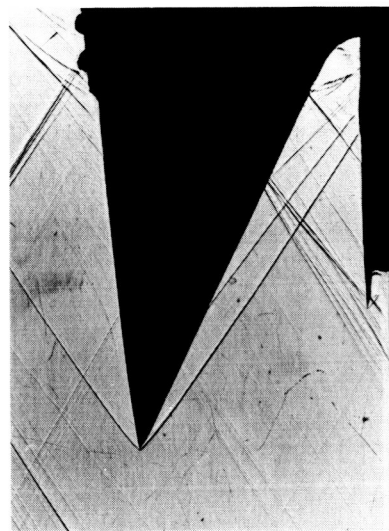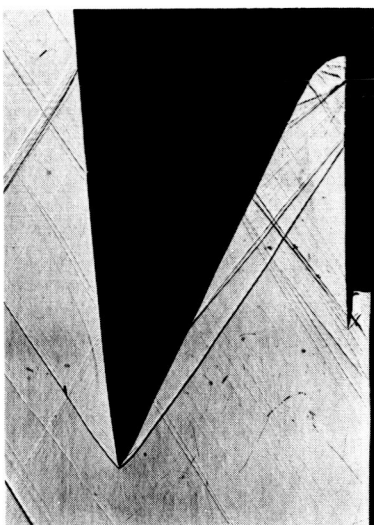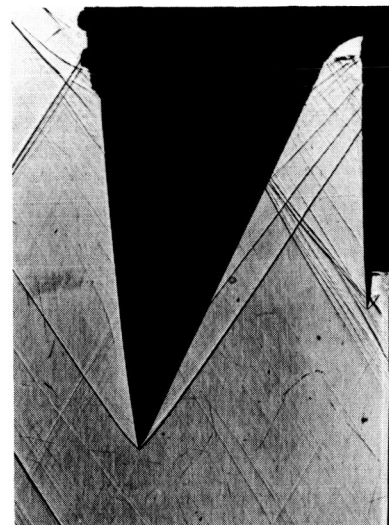
Critical operation

Without compression-surface bleed

Supercritical operation

Critical operation

With 7 compression-surface slots

Supercritical operation

L-57-2703

$M_\infty = 2.02.$

Figure 17.- Shadowgraphs of inlet II-B with and without compression surface bleed.
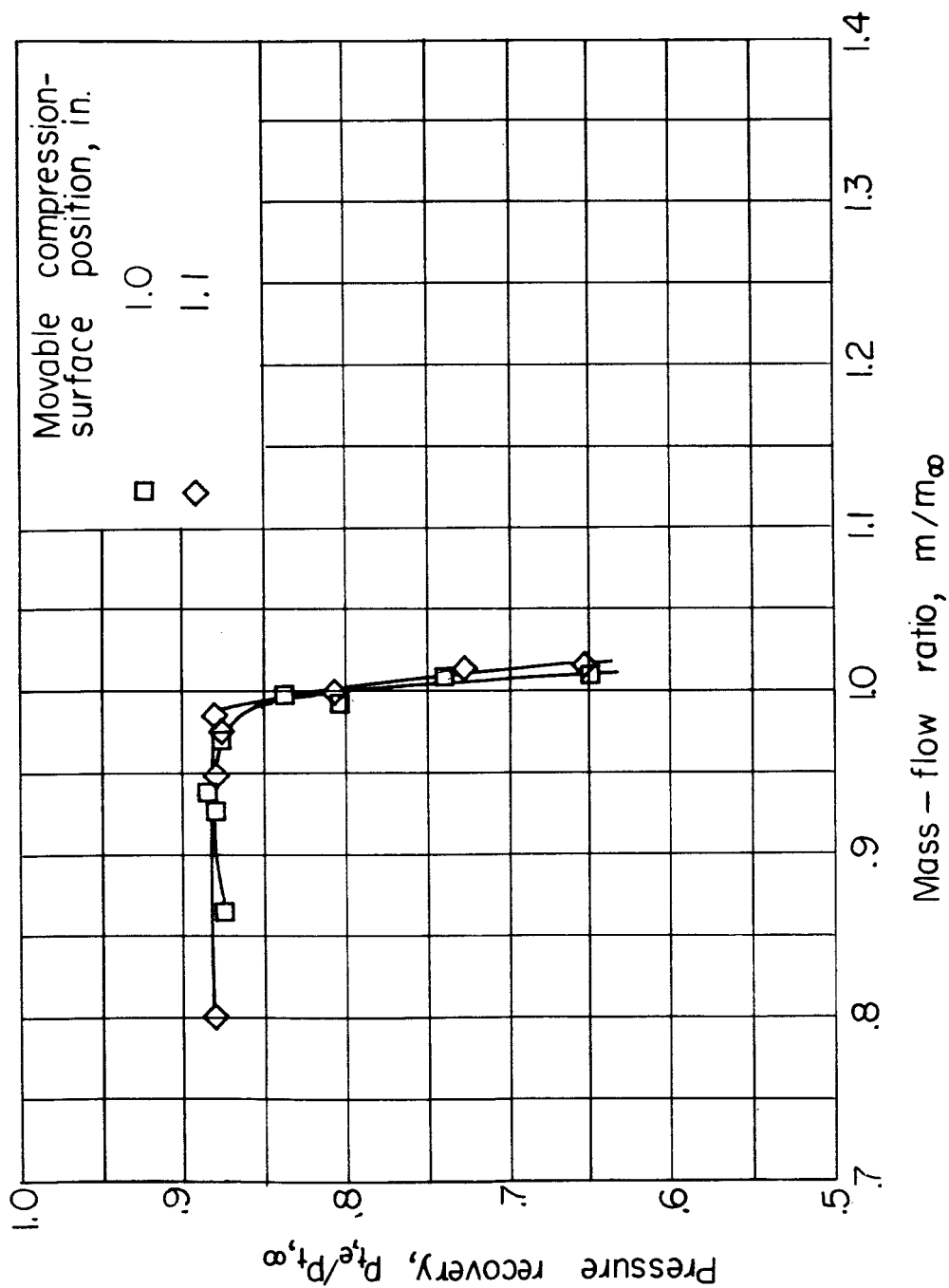
(a) Six compression-surface slots. $M_\infty = 2.02$.

Figure 18.- Performance of inlet III-B showing effect of compression-surface position.
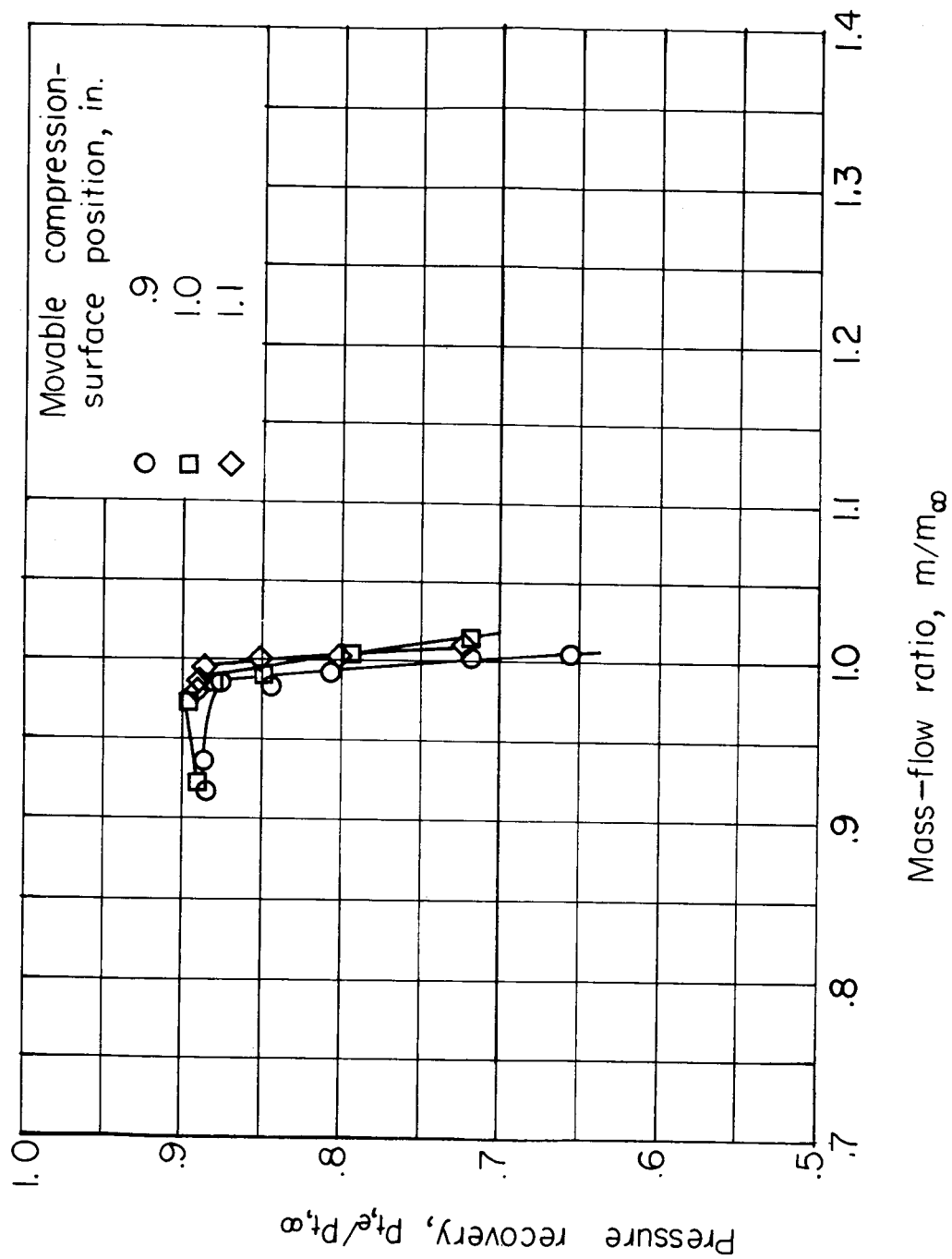
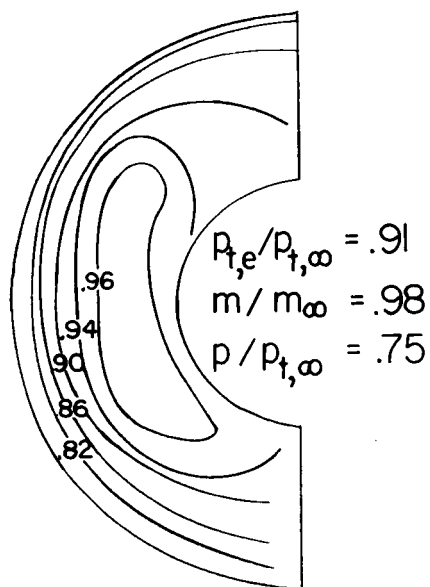(b) Four compression-surface slots. $M_\infty = 2.02$.

Figure 18.- Continued.

(c) Four compression-surface slots. $M_\infty = 1.76$.
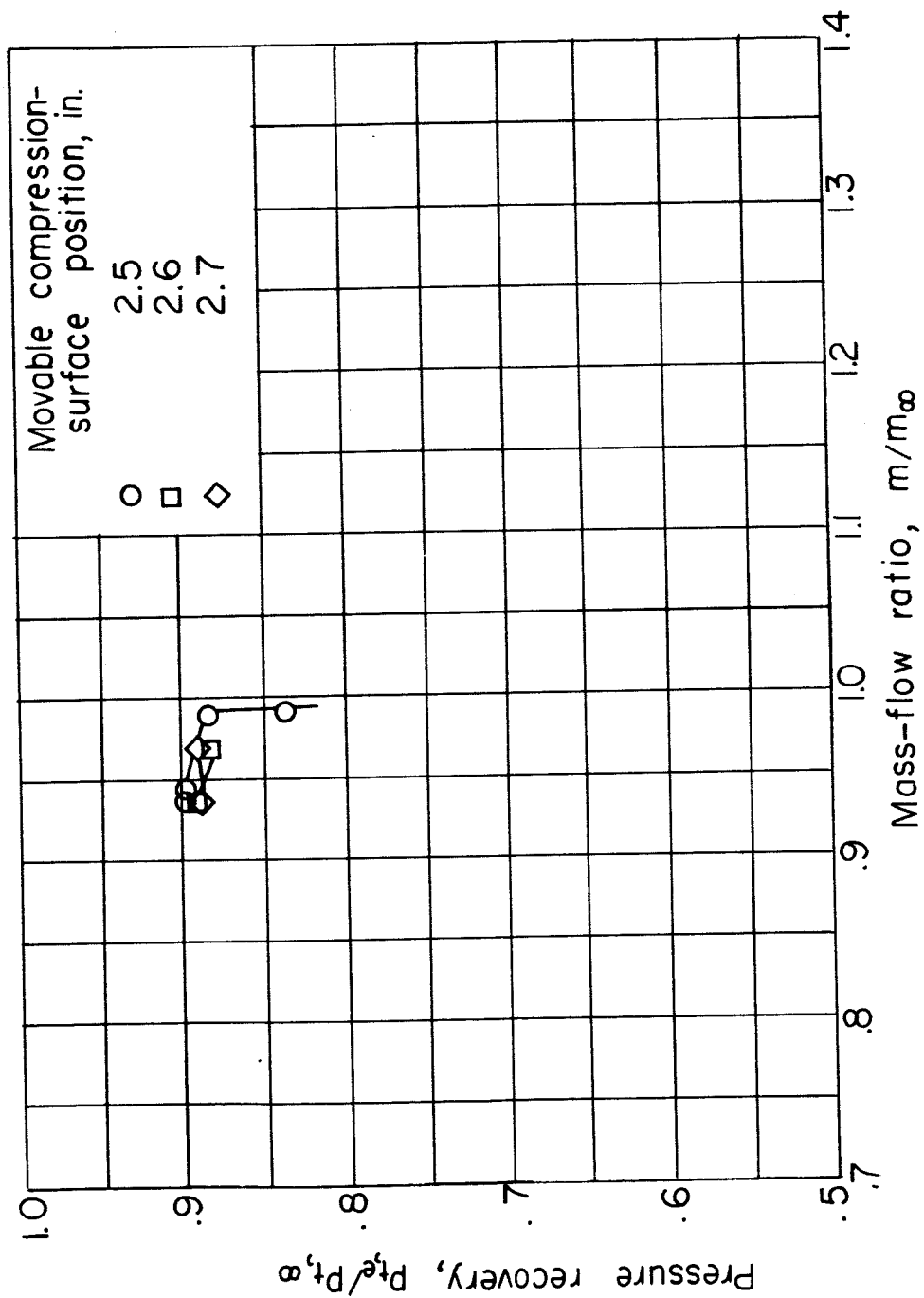
Figure 18.- Continued.
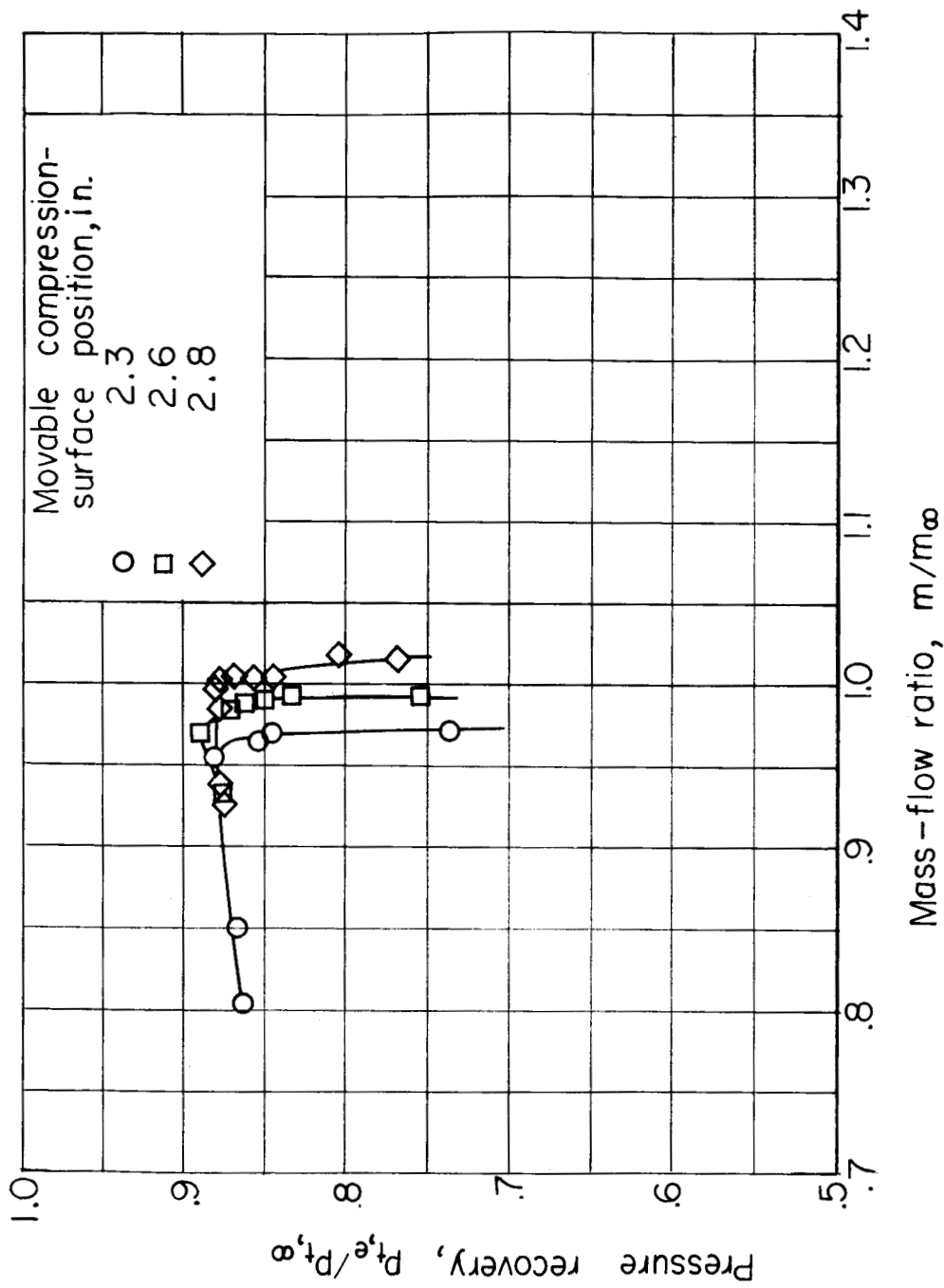
(d) No compression-surface slots. $M_\infty = 1.76$.

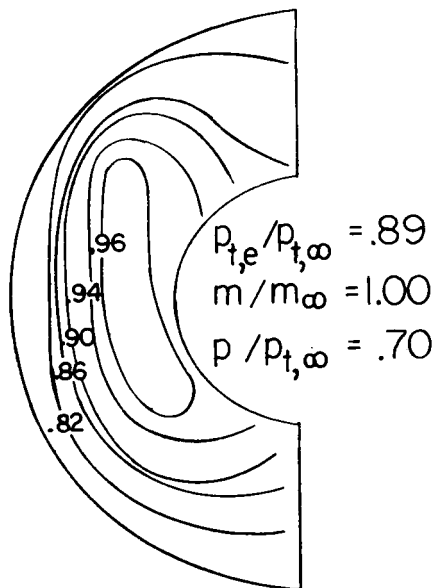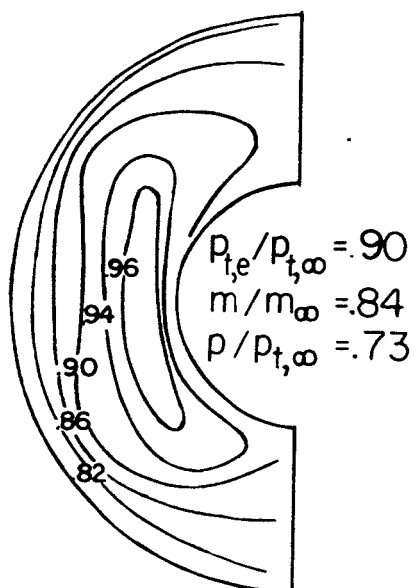Figure 18.- Continued.
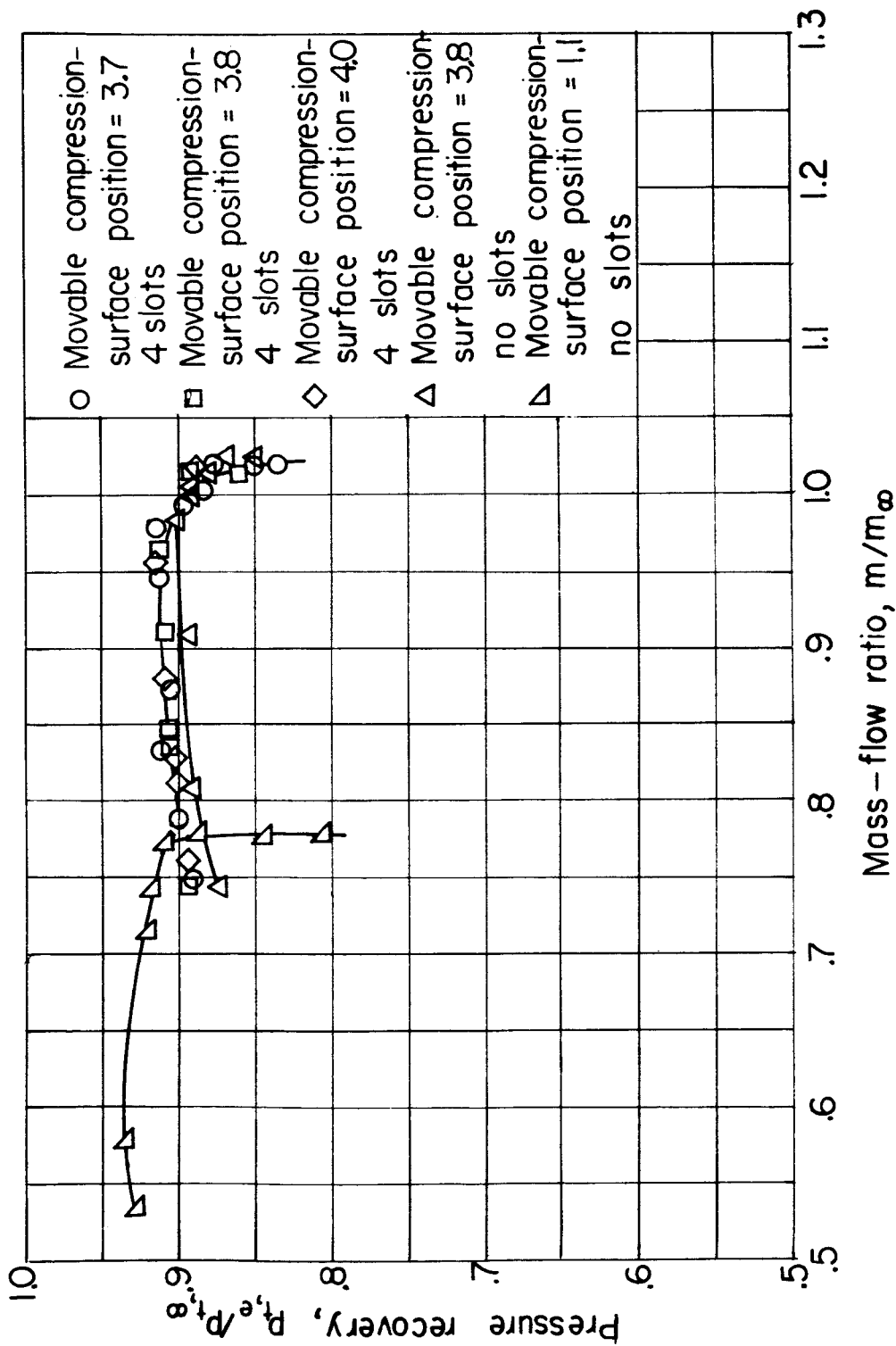
(e) Four compression-surface slots and no compression-surface slots. $M_\infty = 1.60$.

Figure 18.- Concluded.

$p_{t,e}/p_{t,\infty} = .87$

$m/m_\infty = .97$

$p/p_{t,\infty} = .80$

.92

.90

.88

.86

.86

Compression — surface position = 1.0

$p_{t,e}/p_{t,\infty} = .88$

$m/m_\infty = .98$

$p/p_{t,\infty} = .80$

.94

.92

.90

.88

.86

.84
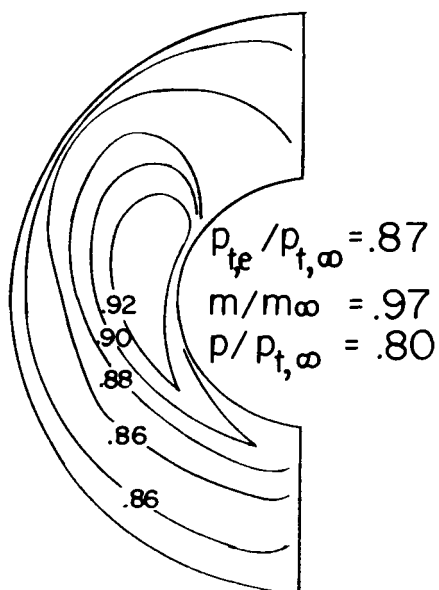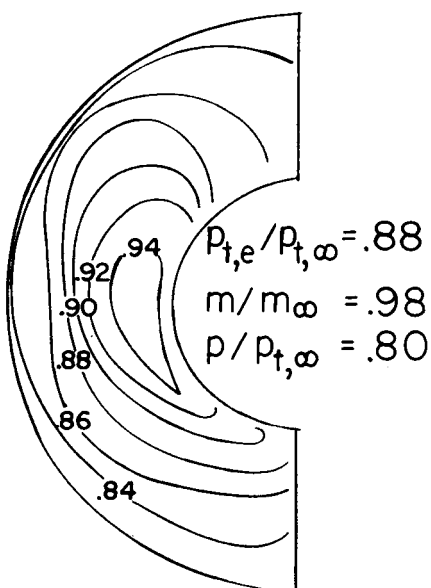
Compression — surface position = 1.1

(a) Six compression-surface slots. $M_\infty = 2.02$.

Figure 19.- Total-pressure distributions of inlet III-B.

$p_{t,e}/p_{t,\infty} = .88$
$m/m_\infty = .99$
$p/p_{t,\infty} = .81$

.92
.90
.88
.86

Compression — surface
position = .9

$p_{t,e}/p_{t,\infty} = .89$
$m/m_\infty = .97$
$p/p_{t,\infty} = .80$

.94
.92
.90
.88
.86

Compression — surface
position = 1.0

$p_{t,e}/p_{t,\infty} = .88$
$m/m_\infty = 1.00$
$p/p_{t,\infty} = .81$

.94
.92
.90
.88
.86

Compression — surface
position = 1.1
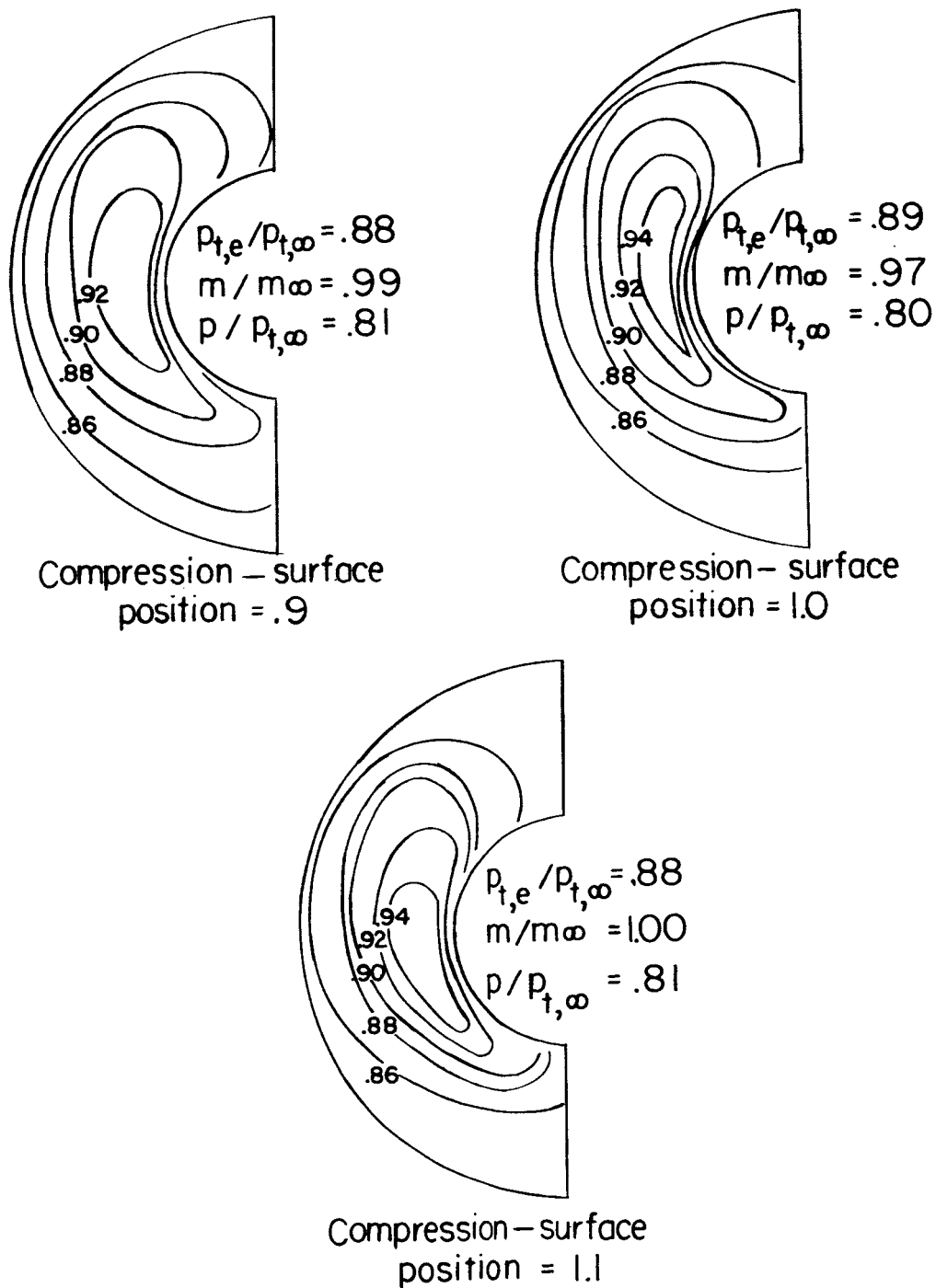
(b) Four compression-surface slots. $M_\infty = 2.02$.

Figure 19.- Continued.
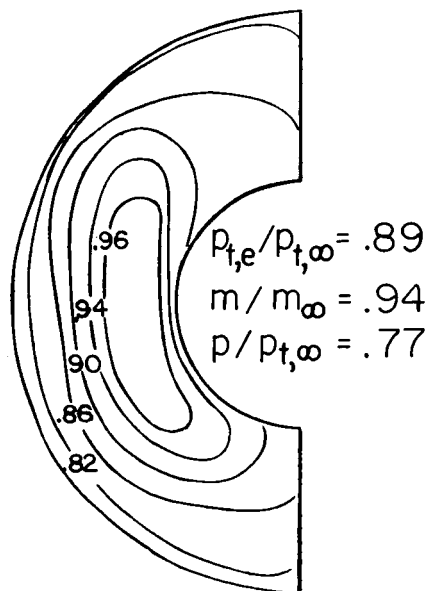
$p_{t,e}/p_{t,\infty} = .89$
$m/m_\infty = .94$
$p/p_{t,\infty} = .77$

.96
.94
.90
.86
.82

Compression – surface
position = 2.5

$p_{t,e}/p_{t,\infty} = .88$
$m/m_\infty = .93$
$p/p_{t,\infty} = .76$

.94
.90
.86
.82

Compression – surface
position = 2.6

$p_{t,e}/p_{t,\infty} = .89$
$m/m_\infty = .96$
$p/p_{t,\infty} = 76$

.96
.94
.90
.86
.82
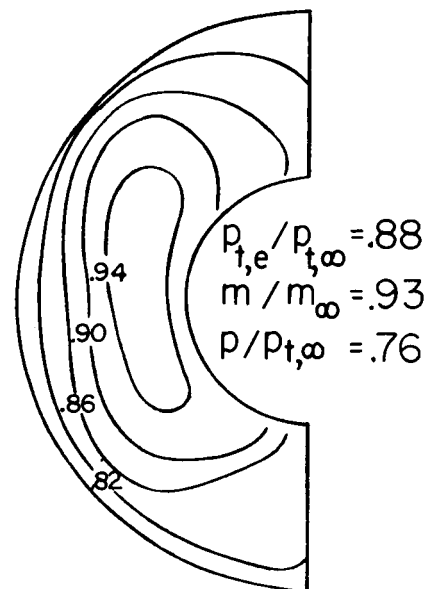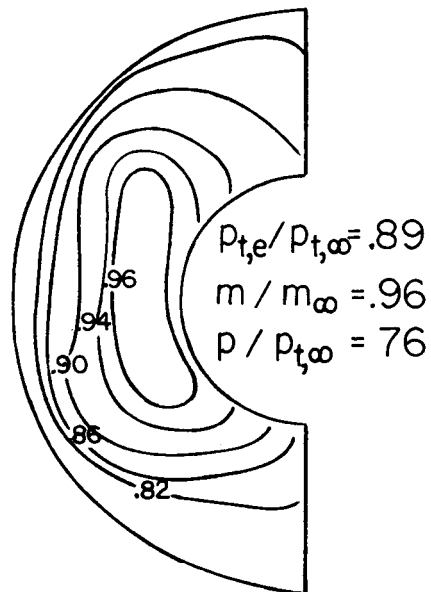
Compression – surface
position = 2.7

(c) Four compression-surface slots. $M_\infty = 1.76$.
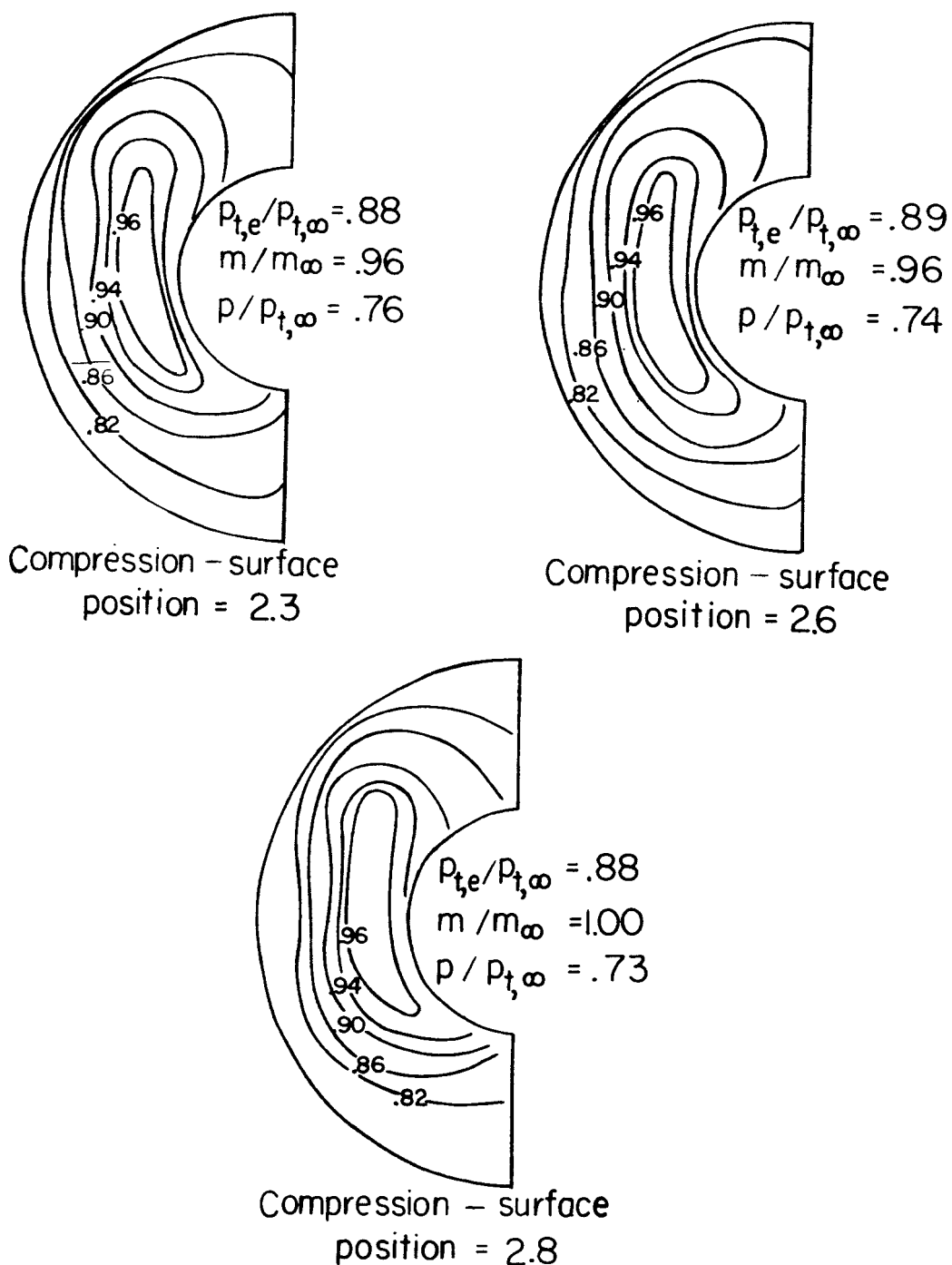
Figure 19.- Continued.

DECLASSIFIED

$p_{t,e}/p_{t,\infty} = .88$
$m/m_\infty = .96$
$p/p_{t,\infty} = .76$

Compression – surface
position = 2.3

$p_{t,e}/p_{t,\infty} = .89$
$m/m_\infty = .96$
$p/p_{t,\infty} = .74$

Compression – surface
position = 2.6

$p_{t,e}/p_{t,\infty} = .88$
$m/m_\infty = 1.00$
$p/p_{t,\infty} = .73$

Compression – surface
position = 2.8

(d) No compression-surface slots. $M_\infty = 1.76$.

Figure 19.- Continued.

$$p_{t,e}/p_{t,\infty} = .91$$
$$m/m_\infty = .98$$
$$p/p_{t,\infty} = .75$$

.96
.94
.90
.86
.82

Compression — surface
position = 3.7

$$p_{t,e}/p_{t,\infty} = .89$$
$$m/m_\infty = 1.00$$
$$p/p_{t,\infty} = .72$$

.96
.94
.90
.86
.82

Compression — surface
position = 3.8

$$p_{t,e}/p_{t,\infty} = .89$$
$$m/m_\infty = 1.00$$
$$p/p_{t,\infty} = .70$$

.96
.94
.90
.86
.82

Compression — surface
position = 4.0

(e) Four compression-surface slots. $M_\infty = 1.60$.

Figure 19.- Continued.

$p_{t,e}/p_{t,\infty} = .90$
$m/m_\infty = .84$
$p/p_{t,\infty} = .73$

.96
.94
.90
.86
.82

Compression-surface position = 3.8

$p_{t,e}/p_{t,\infty} = .91$
$m/m_\infty = .77$
$p/p_{t,\infty} = .81$

.96
.94
.90
.86

Compression - surface position = 1.1

(f) No compression-surface slots. $M_\infty = 1.60$.

Figure 19.- Concluded.
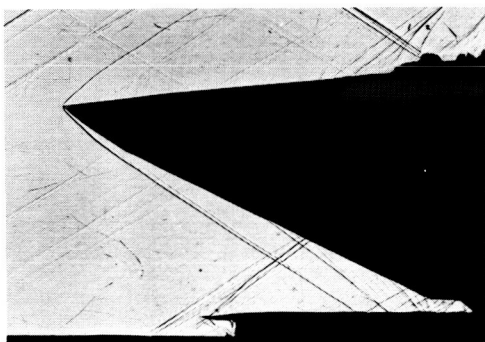
Supercritical operation
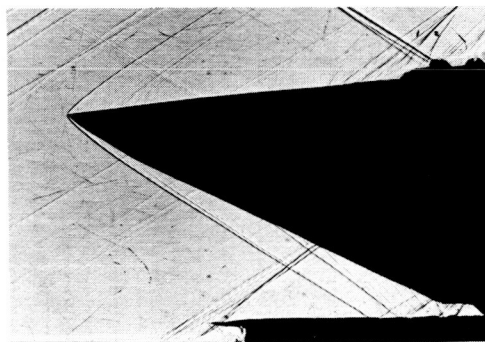
Maximum pressure recovery

$M_\infty = 2.02$
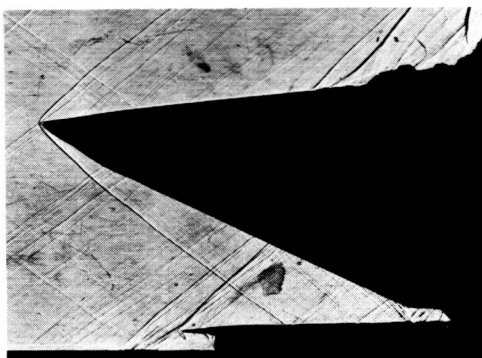
Supercritical operation
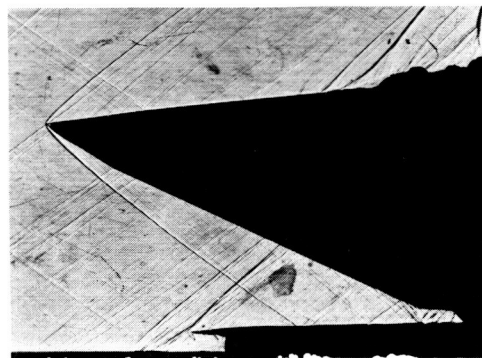
Maximum pressure recovery

$M_\infty = 1.76$
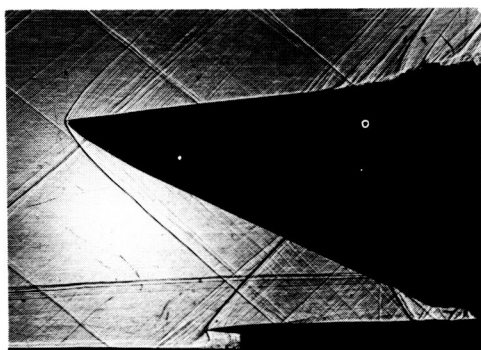
Supercritical operation
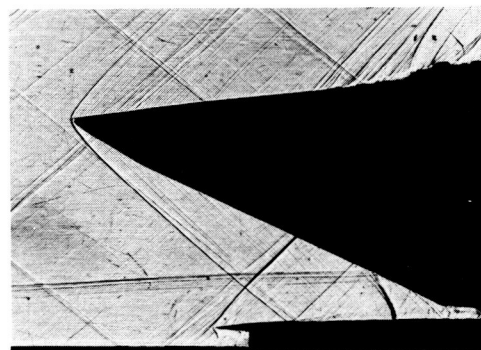
Maximum pressure recovery

$M_\infty = 1.60$

L-57-2704

Figure 20.- Shadowgraphs of inlet III-B with four compression-surface slots.
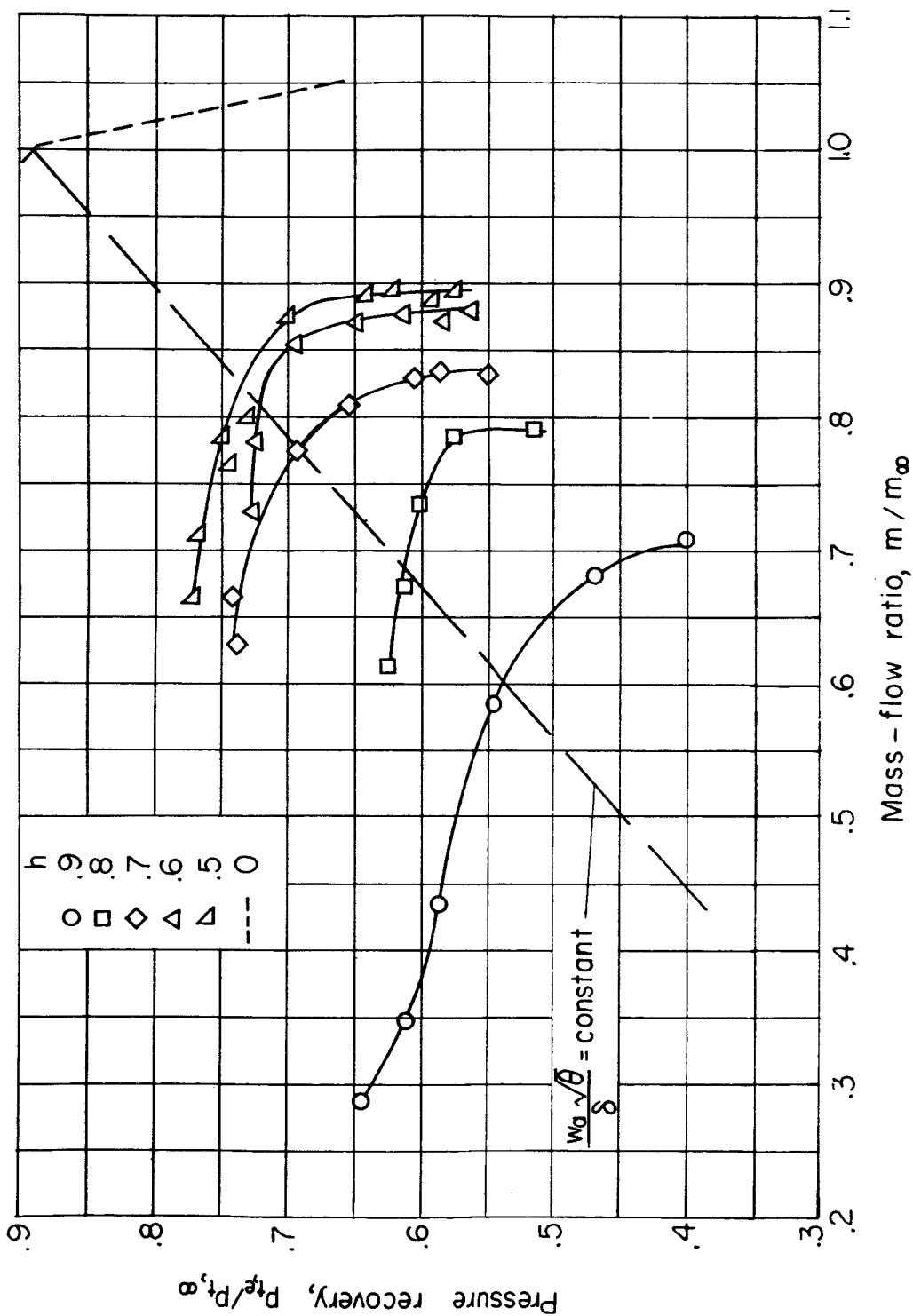
(a) Inlet II-B with seven compression-surface slots. $M_\infty = 2.02$.

Figure 21.- Performance of buzz suppressors.
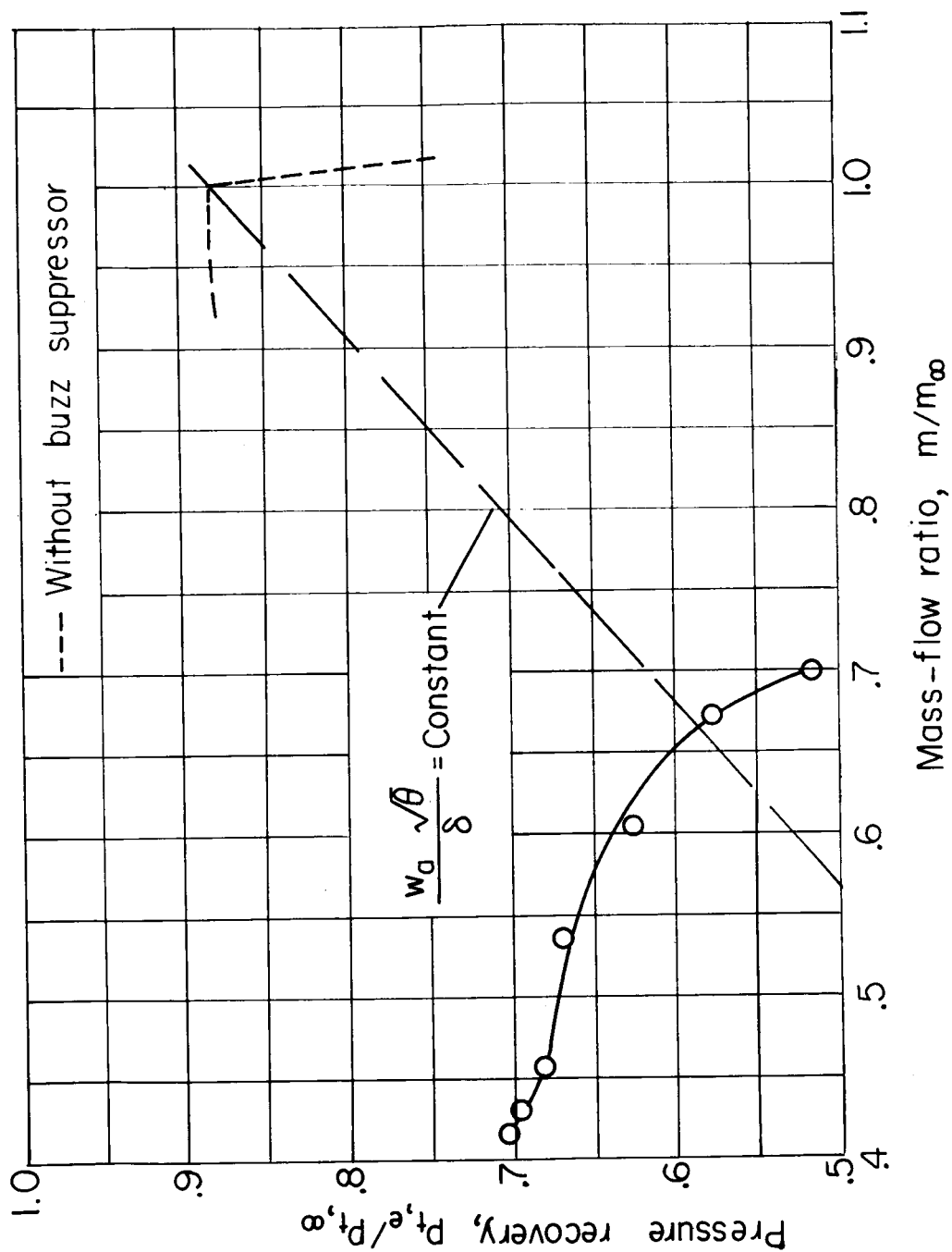
(b) Inlet III-B with seven compression-surface slots. $M_\infty = 1.76$; $h = 0.9$ inch.

Figure 21.- Concluded.

$$p_{t,e}/p_{t,\infty} = .54$$
$$m/m_\infty = .59$$
$$p/p_{t,\infty} = .49$$

.58
.56
.54
.52

h = .9

.66
.62
.60
.58
.62

$$p_{t,e}/p_{t,\infty} = .61$$
$$m/m_\infty = .67$$
$$p/p_{t,\infty} = .54$$

h = .8

.74
.72
.70
.68

$$p_{t,e}/p_{t,\infty} = .69$$
$$m/m_\infty = .77$$
$$p/p_{t,\infty} = .55$$

h = .7

.72
.70
.68
.66

$$p_{t,e}/p_{t,\infty} = .69$$
$$m/m_\infty = .86$$
$$p/p_{t,\infty} = .62$$

h = .6
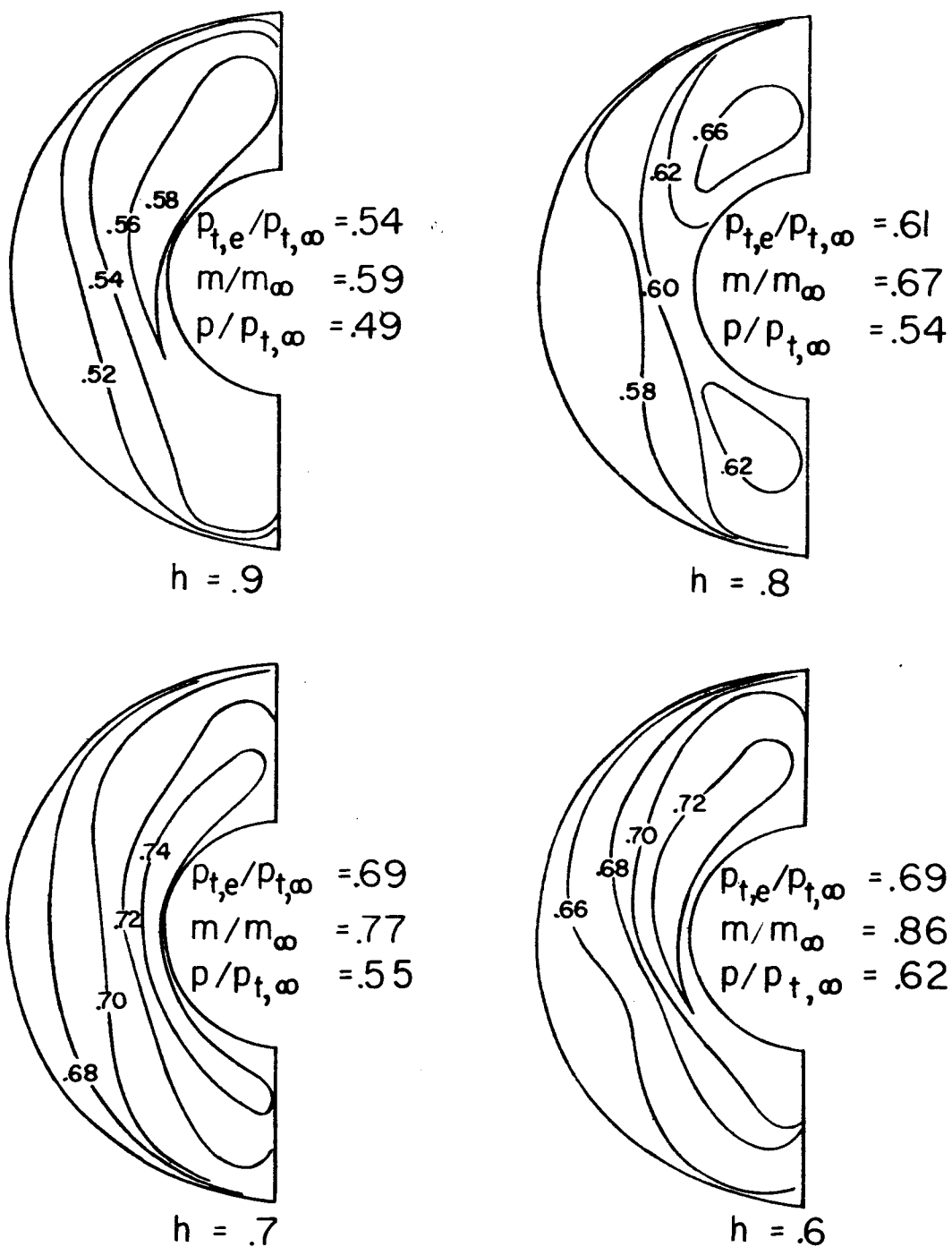
(a) Inlet II-B with seven compression-surface slots. $M_\infty = 2.02$.

Figure 22.- Total-pressure distribution of inlet with buzz suppressors.

$p_{t,e}/p_{t,\infty} = .58$

$m/m_\infty = .67$

$p/p_{t,\infty} = .46$

.66
.62
.58
.54
.50
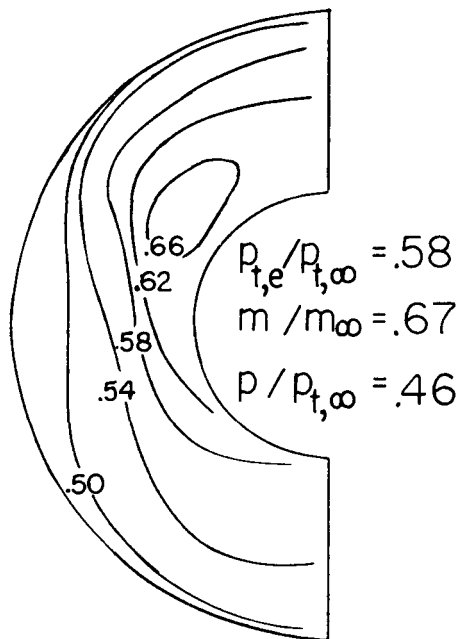
(b) Inlet III-B with seven compression-surface slots. $M_\infty = 1.76$; h = 0.9 inch.

Figure 22.- Concluded.
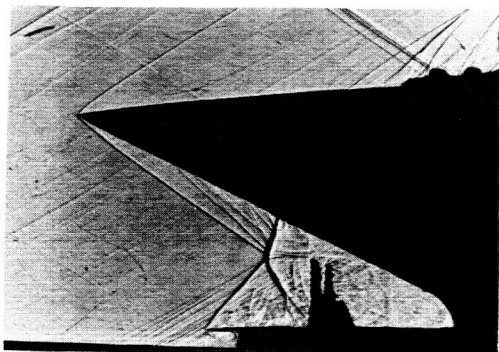
Supercritical operation
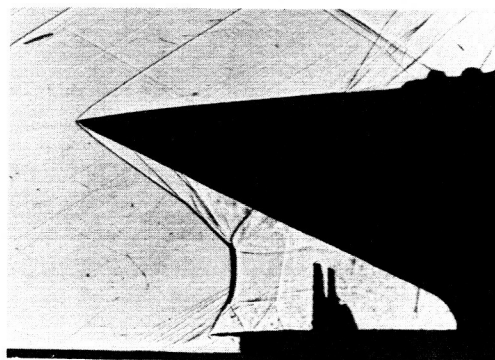
Lowest stable mass flow

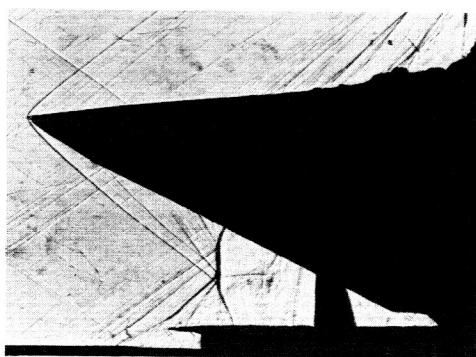Inlet II-B; M_∞ = 2.02; buzz suppressors fully extended; h = 0.9 in.
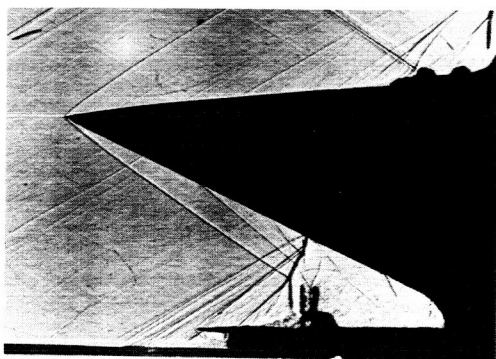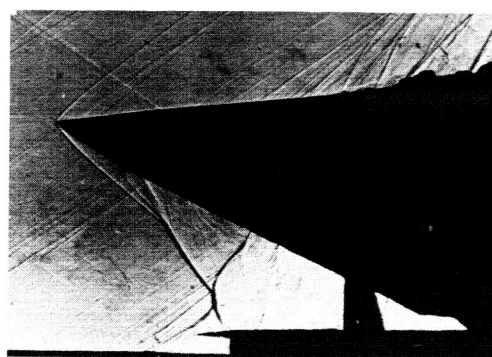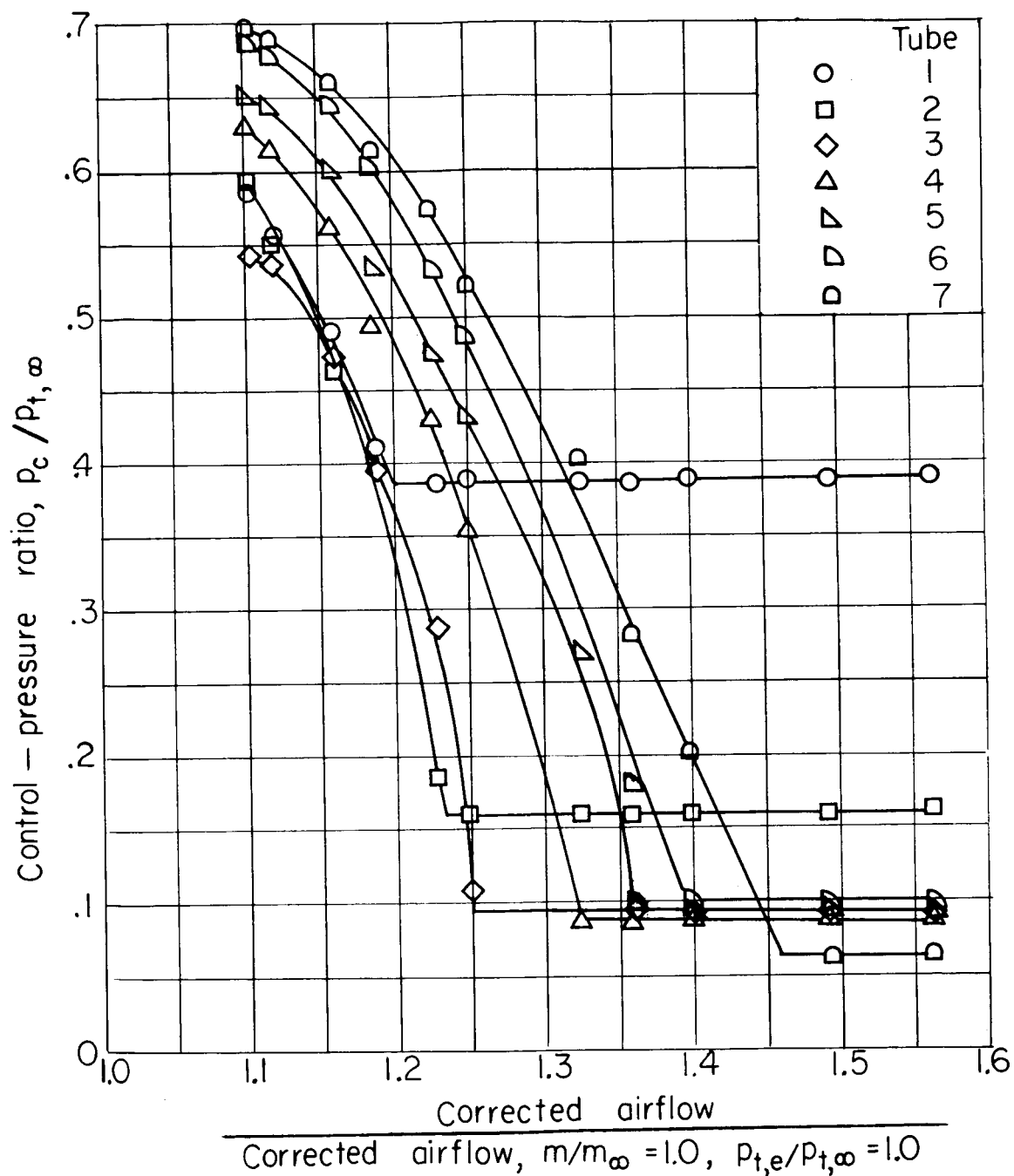
Supercritical operation
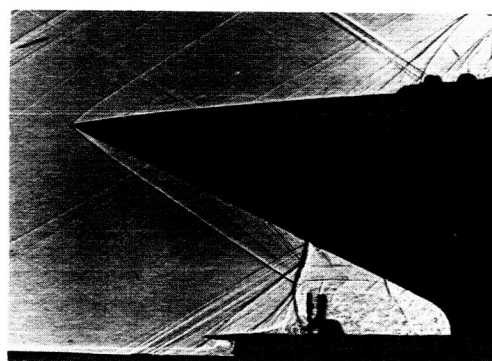
Lowest stable mass flow

Inlet II-B; M_∞ = 2.02, buzz suppressors partially extended; h = 0.6 in.

Supercritical operation

Lowest stable mass flow

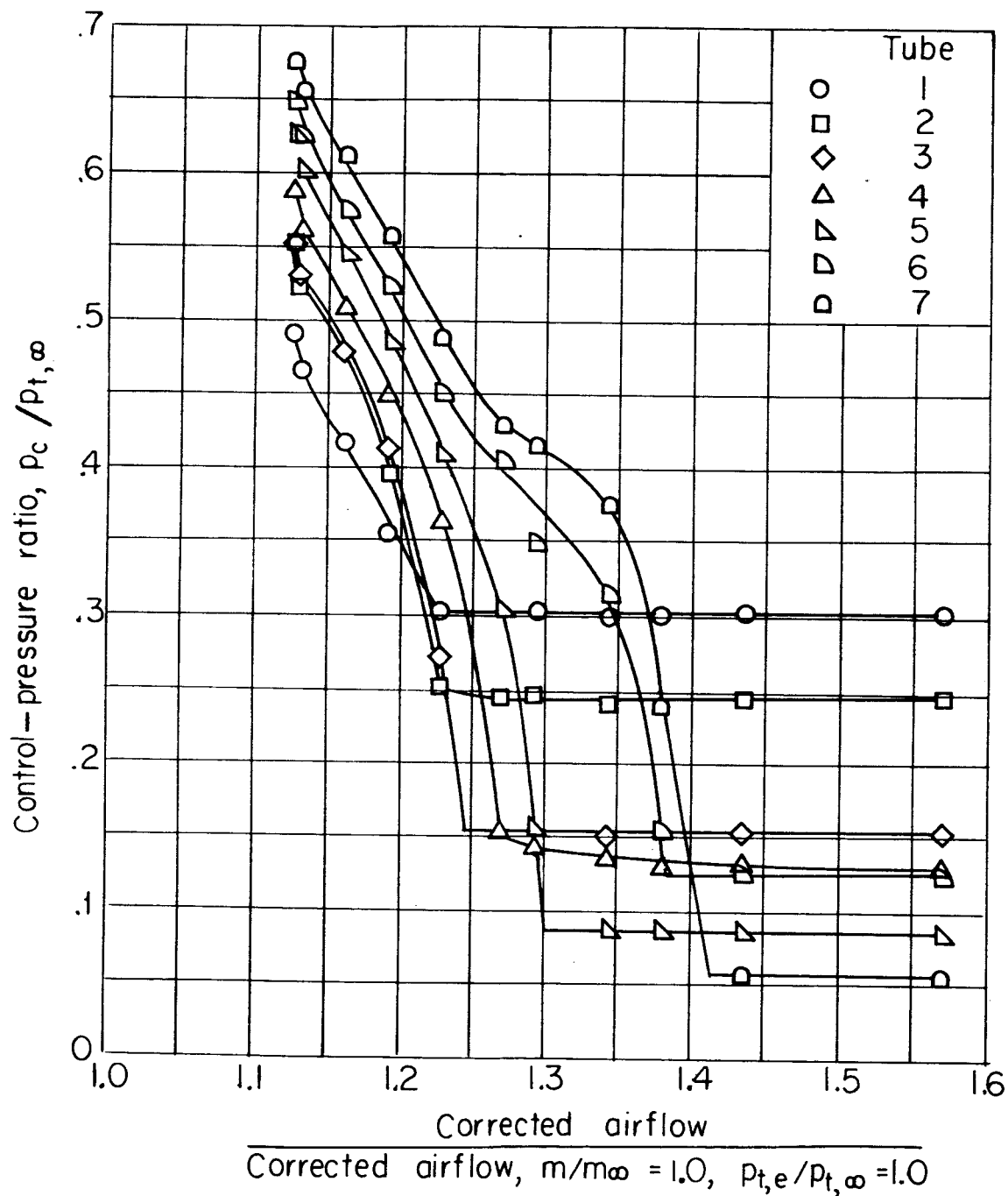Inlet III-B; M_∞ = 1.76; buzz suppressors fully extended; h = 0.9 in.

L-57-2705

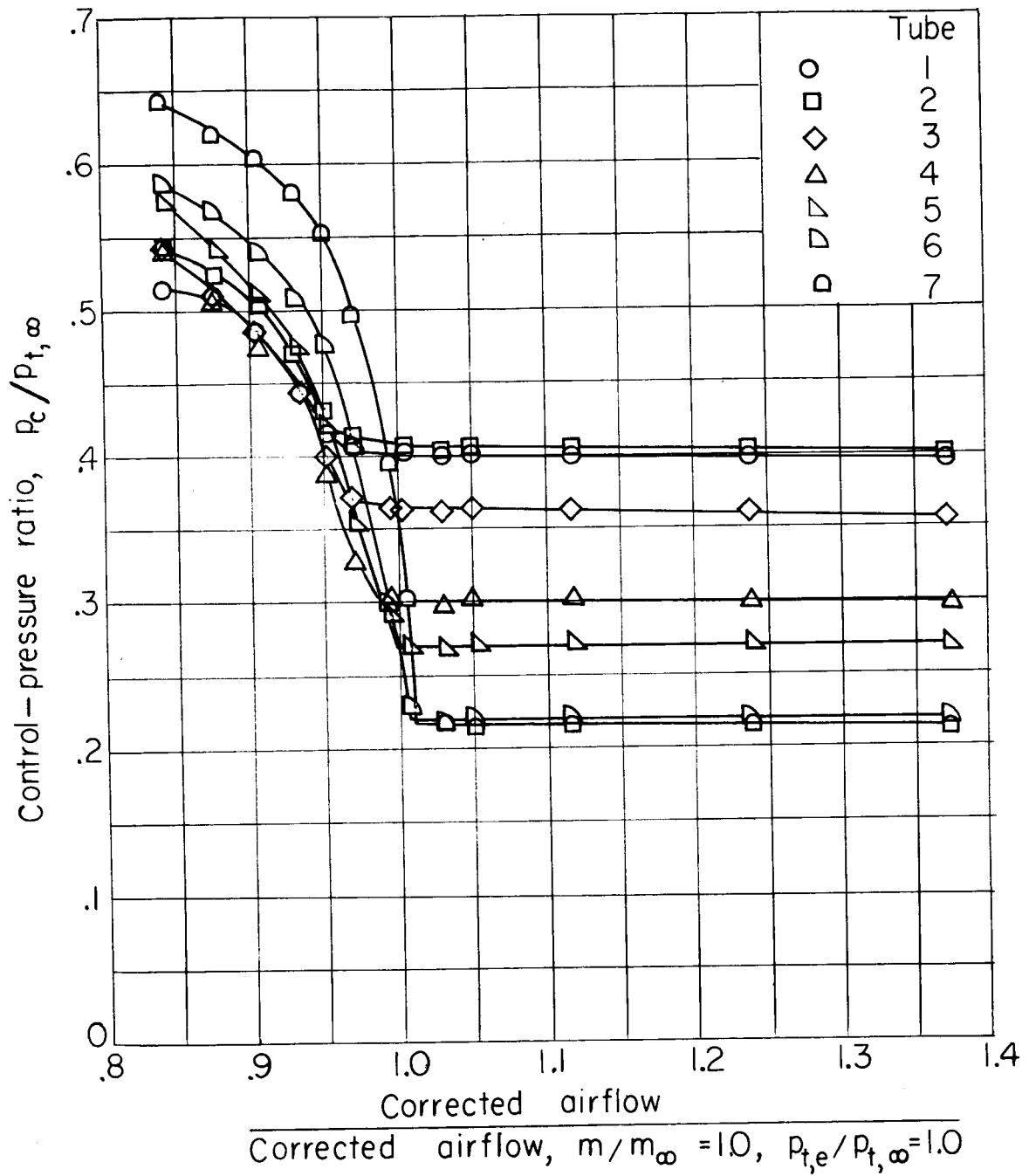Figure 23.- Shadowgraphs of inlet with buzz suppressors and seven compression-surface slots.

(a) Inlet II-B with 7 compression-surface slots. $M_\infty = 2.02$.

Figure 24.- Characteristics of rearward-facing control tubes located on inboard wall.

Corrected airflow

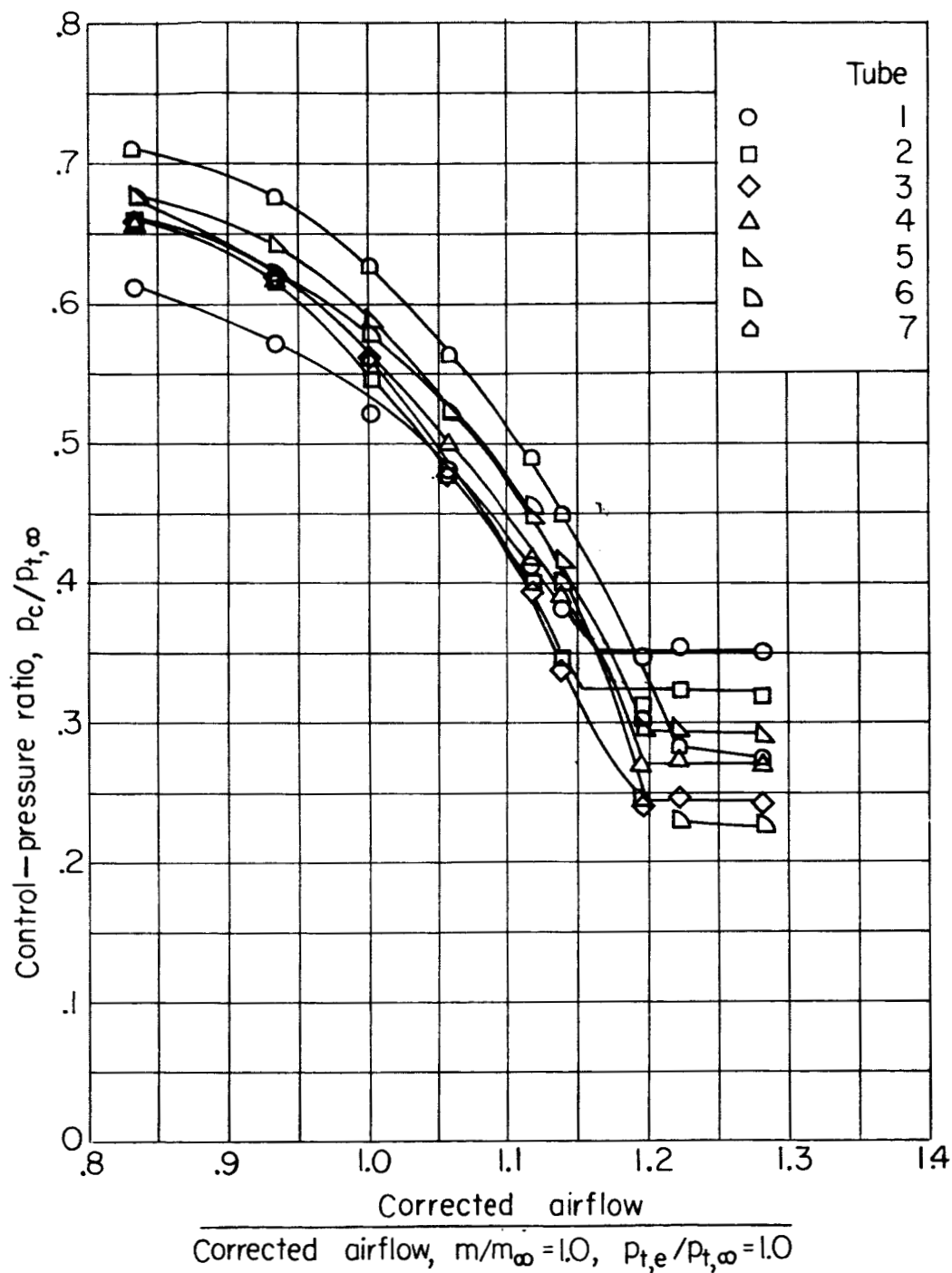Corrected airflow, $m/m_\infty = 1.0$, $p_{t,e}/p_{t,\infty} = 1.0$

(b) Inlet III-B with four compression-surface slots. $M_\infty = 2.02$.

Figure 24.- Continued.

(c) Inlet III-B with four compression-surface slots. $M_\infty = 1.76$.
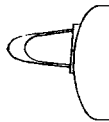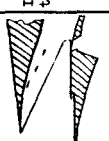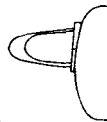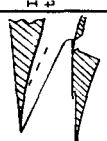
Figure 24.- Continued.

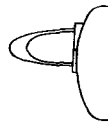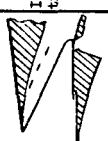(d) Inlet III-B with four compression-surface slots. $M_\infty = 1.60$.

Figure 24.- Concluded.

NOTES: (1) Reynolds number is based on the diameter of a circle with the same area as that of the capture area of the inlet.

(2) The symbol * denotes the occurrence of buzz.

Description				Test parameters								Performance		
Report and facility	Configuration	Number of oblique shocks	Type of boundary-layer control	Free-stream Mach number	Reynolds number × 10⁻⁶	Angle of attack, deg	Angle of yaw, deg	Drag	Inlet-flow profile	Discharge-flow profile	Flow picture	Maximum total-pressure recovery	Mass-flow ratio	Remarks
CONFID. RM L57G15 Langley Gas Dynamics		Isentropic	Fuselage diverter plus bleed slots on diverter and compression surface	2.02	4.80	0	0			✓	✓	0.90	1.00 to 0.99*	Stable mass-flow range extended to 0.30 and 0.42 for M = 2.02 and 1.76, respectively, by use of buzz suppressor.
				1.76	5.00	0	0			✓	✓	.88	1.00 to 0.80*	
				1.60	5.25	0	0			✓	✓	.90	1.00 to 0.75*	
CONFID. RM L57G15 Langley Gas Dynamics		Isentropic	Fuselage diverter plus bleed slots on diverter and compression surface	2.02	4.80	0	0			✓	✓	0.90	1.00 to 0.99*	Stable mass-flow range extended to 0.30 and 0.42 for M = 2.02 and 1.76, respectively, by use of buzz suppressor.
				1.76	5.00	0	0			✓	✓	.88	1.00 to 0.80*	
				1.60	5.25	0	0			✓	✓	.90	1.00 to 0.75*	
CONFID. RM L57G15 Langley Gas Dynamics		Isentropic	Fuselage diverter plus bleed slots on diverter and compression surface	2.02	4.80	0	0			✓	✓	0.90	1.00 to 0.99*	Stable mass-flow range extended to 0.30 and 0.42 for M = 2.02 and 1.76, respectively, by use of buzz suppressor.
				1.76	5.00	0	0			✓	✓	.88	1.00 to 0.80*	
				1.60	5.25	0	0			✓	✓	.90	1.00 to 0.75*	
CONFID. RM L57G15 Langley Gas Dynamics		Isentropic	Fuselage diverter plus bleed slots on diverter and compression surface	2.02	4.80	0	0			✓	✓	0.90	1.00 to 0.99*	Stable mass-flow range extended to 0.30 and 0.42 for M = 2.02 and 1.76, respectively, by use of buzz suppressor.
				1.76	5.00	0	0			✓	✓	.88	1.00 to 0.80*	
				1.60	5.25	0	0			✓	✓	.90	1.00 to 0.75*	

Bibliography

These strips are provided for the convenience of the reader and can be removed from this report to compile a bibliography of NACA inlet reports. This page is being added only to inlet reports and is on a trial basis.